NOVA SCHOOL OF SCIENCE & TECHNOLOGY

DEPARTMENT OF PHYSICS

MARGARIDA MARIA RODRIGUES BARATA

BsC in Biomedical Engineering

# NATURE-DERIVED CONDUCTIVE SCAFFOLDS FOR THERAPEUTIC APPLICATIONS

MASTER IN BIOMEDICAL ENGINEERING

NOVA University Lisbon
September, 2023

NOVA SCHOOL OF SCIENCE & TECHNOLOGY

DEPARTMENT OF PHYSICS

# NATURE-DERIVED CONDUCTIVE SCAFFOLDS FOR THERAPEUTIC APPLICATIONS

MARGARIDA MARIA RODRIGUES BARATA

BsC in Biomedical Engineering

**Adviser:** Henrique Martiniano Vazão de Almeida
*Researcher, CENIMAT|i3N*

**Examination Committee:**

**Chair:** Célia Maria Reis Henriques
*Associated Professor, FCT-NOVA*

**Rapporteur:** Tânia Sofia dos Santos Vieira
*Assistant Researcher, FCT-NOVA*

**Adviser:** Henrique Martiniano Vazão de Almeida
*Researcher, CENIMAT|i3N*

MASTER IN BIOMEDICAL ENGINEERING

NOVA University Lisbon
September, 2023

**Nature-derived Conductive Scaffolds for Therapeutic Applications**

*Para a minha família.*

# Acknowledgements

A realização desta dissertação de mestrado não teria sido possível sem a colaboração e apoio de várias pessoas e instituições, a quem estendo o meu profundo agradecimento. Em primeiro lugar, gostaria de agradecer à Professora Elvira Fortunato, por me permitir trabalhar neste Centro de Investigação de Excelência, o CENIMAT|i3N na FCT-NOVA.

Expresso também o meu sincero agradecimento ao meu orientador Dr. Henrique Vazão de Almeida pela confiança e partilha de conhecimentos durante estes meses, mantendo sempre uma postura positiva e motivadora. Admiro muito o seu trabalho, curiosidade e incansável busca pela excelência! Muito obrigado pelo seu acompanhamento constante, por todas as reuniões produtivas, por se preocupar com o meu bem-estar e satisfação durante o desenvolvimento deste projeto e pelo feedback constante que sempre me deu. Agradeço também aos responsáveis pelo CEDOC|iNOVA4Health na NOVA Medical School por me proporcionarem a oportunidade de realizar nas suas instalações os ensaios de cultura celular, e, especialmente ao Dr. José Inácio pela sua disposição e ajuda constantes.

Quero também agradecer à Maria Morais pela sua disponibilidade, sugestões valiosas desde o início do projeto, boa disposição e por todas as vezes que me acompanhou nas sessões de Espetroscopia de Raman. Ao Tomás Pinheiro, expresso a minha gratidão pela sua prontidão a me ajudar a operar o sistema de laser e por todas as vezes que reunimos para apresentar novos resultados. O meu agradecimento à Cláudia Pereira por toda a disponibilidade e ajuda para realizar os ensaios celulares e por apresentar soluções alternativas para alguns obstáculos que iam surgindo. Agradeço também ao Tomás Calmeiro pelas várias ocasiões em que realizou o coating das minhas amostras. Estendo o meu agradecimento à Alexandra Gonçalves, Marta e toda a equipa do CENIMAT pela forma como me integraram e por terem contribuído para um ambiente laboratorial alegre e acolhedor.

À Filipa, Carolina, Mariana, Catarina e Rabia, as minhas colegas de laboratório, o meu sincero agradecimento pela entreajuda, motivação constante e pelos bons momentos partilhados. Aos meus queridos amigos de Engenharia Biomédica, Irina, Joana, Marta, Dania, Beatriz e António, estendo o meu profundo agradecimento pelo vosso apoio

contínuo, amizade e pelas nossas conversas inspiradoras. Agradeço às minhas colegas Maria e Susana pela oportunidade de fazer parte da Presidência convosco do Núcleo de Biomédica da NOVA e que apesar de todos os desafios conseguimos superá-los em conjunto. Agradeço à Sara, tanto pelos ensinamentos como pela motivação que sempre me deu. Sinto-me muito orgulhosa por ter realizado a II Edição do Encontro de Universitários Madeirenses com ela, sem dúvida uma das experiências mais desafiantes até hoje!

Aos meus pais que sempre acreditaram no meu potencial, pelo vosso amor e valores que me transmitiram e que moldaram a pessoa que sou hoje. Obrigada à minha avó Caetana por me relembrar continuamente da importância do trabalho árduo na conquista dos objetivos. Um agradecimento especial ao meu namorado Nuno, pelo apoio durante a elaboração da tese e por me fazer sempre acreditar que através da determinação, persistência, consistência e foco, é apenas "uma questão de tempo" para alcançar o sucesso.

Esta experiência da qual me orgulho imenso trouxe-me uma enorme aprendizagem na área de Engenharia de Tecidos Cardíacos. Estou grata pela oportunidade de ter realizado este projeto e sinto-me inspirada desde o primeiro dia que ouvi a explicação sobre o propósito do mesmo. Espero que esta tese sirva de porta de entrada para futuros trabalhos e que tenha um impacto significativo na Ciência. Rumo ao futuro!

*"If you want to go fast, go alone, if you want to go far, go together." (African Proverb)*

# Abstract

Cardiovascular Diseases (CVD), currently considered the leading cause of death worldwide, highlight the imminent need for innovative therapies in the treatment of cardiac pathologies. In this study, Cardiac Tissue Engineering (CTE) was highlighted as a promising approach, featuring the potential of Induced Pluripotent Stem Cell-Derived Cardiomyocytes (iPSC-CMs). One of the main challenges was the difficulty for many substrates to induce cellular maturation equivalent to that of an adult human heart. For this reason, this research consisted of developing substrates based on gelatin and conductive materials, such as Laser-Induced Graphene (LIG), which simulate the characteristics of the natural myocardial microenvironment. LIG is obtained by laser irradiating suitable carbon-based precursors by photoconverting $sp^3$ carbon atoms into $sp^2$ carbon atoms, resulting in a three-dimensional structure of highly conductive porous graphene. Thus, two groups that served as substrates for LIG were analyzed: (a) one containing gelatin and sodium tetraborate decahydrate and (b) another composed of gelatin, genipin and sodium tetraborate decahydrate. The mechanical and electrical properties of the films were studied before and after immersion in a solution of 1-Ethyl-3-(3-dimethylaminopropyl)carbodiimide (EDC)-N-Hydroxysuccinimide (NHS). This crosslinking agent has been used to improve the stability of substrates in *in vitro* physiological environments. Out of the substrates analyzed, only the 2 immersed in EDC-NHS were evaluated for their influence on viability, cell proliferation and expression of proteins indicative of the contractile phenotype of iPSC-CMs, namely $\alpha$-Actinin. The results obtained indicate that the substrate containing genipin was promising, exhibiting conductive properties similar to those of human heart tissue, consequently maintaining cell viability and promoting the proliferation and maturation of iPSC-CMs. These cells showed a morphology relatively similar to mature Cardiomyocytes (CMs) and a notable expression of contractile proteins. The genipin film appears as a new proposal in the field of CTE, signaling possible clinical advances in the fight against CVD and representing significant progress in this area.

**Keywords:** Cardiovascular Diseases (CVD), Cardiac Tissue Engineering (CTE), Induced Pluripotent Stem Cell-Derived Cardiomyocytes (iPSC-CMs), Cardiac Extracellular Matrix (ECM), Gelatin, Laser-Induced Graphene (LIG), Genipin, 1-Ethyl-3-(3-dimethylaminopropyl)carbodiimide-N-Hydroxysuccinimide (EDC-NHS).

# Resumo

As doenças cardiovasculares (CVD), consideradas atualmente a principal causa de morte a nível mundial, evidenciam a necessidade iminente de terapias inovadoras no tratamento de patologias cardíacas. Neste estudo, destacou-se a engenharia de tecidos cardíacos (CTE) como uma abordagem promissora, ressaltando o potencial dos cardiomiócitos derivados de células estaminais pluripotentes induzidas (iPSC-CMs). Um dos principais desafios é a dificuldade de muitos substratos induzirem a maturação celular equivalente à de um coração humano adulto. Por esse motivo, esta pesquisa consistiu no desenvolvimento de substratos baseados em gelatina e materiais condutores, como o grafeno induzido por laser (LIG), que simulam as características do microambiente natural miocárdico. O LIG é obtido a partir da irradiação a laser de precursores à base de carbono, convertendo átomos de carbono $sp^3$ em $sp^2$, resultando numa estrutura tridimensional de grafeno poroso altamento condutor. Assim, foram analisados dois grupos que serviram de substrato para o LIG: (a) um contendo gelatina e tetraborato de sódio decahidratado e (b) outro composto por gelatina, genipina e tetraborato de sódio decahidratado. Foram estudadas as propriedades mecânicas e elétricas dos filmes antes e após imersão numa solução de 1-Etil-3-(3-dimetilaminopropil)carbodiimida-N-Hidroxisuccinimida (EDC-NHS); este agente reticulante foi utilizado para melhorar a estabilidade dos substratos em ambientes fisiológicos *in vitro*. Dos substratos analisados, apenas os 2 imersos em EDC-NHS foram avaliados quanto à sua influência na viabilidade, proliferação celular e expressão das proteínas indicativas do fenótipo contrátil dos iPSC-CMs, nomeadamente a $\alpha$-Actinina. Os resultados obtidos indicam que o substrato contendo genipina revelou-se promissor, exibindo propriedades condutoras semelhantes às do tecido cardíaco humano, manteve a viabilidade celular e promoveu a proliferação e maturação dos iPSC-CMs. Estas células apresentaram uma morfologia relativamente semelhante à dos cardiomiócitos (CMs) maduros e uma expressão notável de proteínas contráteis. O filme com genipina surge como uma nova proposta no campo da CTE, sinalizando possíveis avanços clínicos no combate às CVD e representando um progresso significativo nesta área.

**Palavras-chave:** Doenças Cardiovasculares (CVD), Engenharia de Tecidos Cardíacos (CTE), Cardiomiócitos derivados de células estaminais pluripotentes induzidas (iPSC-CMs), Matriz Extracelular (ECM) Cardíaca, Gelatina, Grafeno induzido por Laser (LIG), Genipina, 1-Etil-3-(3-dimetilaminopropil)carbodiimida-N-Hidroxisuccinimida (EDC-NHS).

# Contents

# List of Figures

# List of Tables

# Abbreviations

| | |
|---|---|
| **BSA** | Bovine serum albumin |
| **CG** | Collagen-Glycosaminoglycan |
| **CMs** | Cardiomyocytes |
| **CPCs** | Cardiac Progenitor Cells |
| **CTE** | Cardiac Tissue Engineering |
| **CVD** | Cardiovascular Diseases |
| **DAPI** | 4',6-Diamidino-2-phenylindole |
| **DHT** | Dehydrothermal Treatment |
| **ECM** | Extracellular Matrix |
| **EDC** | 1-Ethyl-3-(3-dimethylaminopropyl)carbodiimide |
| **ESCs** | Embryonic Stem Cells |
| **FTIR** | Fourier-transform infrared spectroscopy |
| **hiPSC-CMs** | Human Induced Pluripotent Stem Cell-Derived Cardiomyocytes |
| **hiPSCs** | Human Induced Pluripotent Stem Cells |
| **iPSC-CMs** | Induced Pluripotent Stem Cell-Derived Cardiomyocytes |
| **iPSCs** | Induced Pluripotent Stem Cells |
| **KL/PEO** | Kraft lignin/poly(ethylene oxide) |
| **LIG** | Laser-Induced Graphene |
| **NHS** | N-Hydroxysuccinimide |

| | |
|---|---|
| **PBS** | Phosphate-buffered saline |
| **PCL** | Polycaprolactone |
| **PDMS** | Polydimethylsiloxane |
| **PEG** | Polyethylene Glycol |
| **PEI** | Polyetherimide |
| **PI** | Polyimide |
| **PLA** | Polylactic Acid |
| **PPI** | Pulses per Inch |
| **RFUs** | Relative Fluorescent Units |
| **SD** | Standard Deviation |
| **SEM** | Scanning Electron Microscopy |
| **TE** | Tissue Engineering |
| **WHO** | World Health Organization |

# 1 Introduction

According to the World Health Organization (WHO), CVD are currently the leading cause of death in the world, accounting for about 32% of all global deaths. It is estimated that around 17.9 million people died in 2019 from these diseases [1].

Considering the worrying prevalence of CVD, it is essential to understand the complexity and importance of the human heart, a vital organ for our survival. The heart is among the most complex organs in terms of its functionality in the body, being composed of three layers of tissue that form the wall of the heart. The outer layer is the epicardium, the middle layer is the myocardium, and the inner layer is the endocardium. The thick layer of the myocardium is formed by a highly branched network of individual cardiac muscle cells, the CMs and these are responsible for the involuntary and rhythmic contractions of the heart. Therefore, the cardiovascular system guarantees the necessary blood flow to supply all body tissues with oxygen and nutrients, as well as to adequately eliminate metabolic waste [2].

In this way, CTE has directed its research towards finding solutions to combat CVD, thus exploring the potential of Induced Pluripotent Stem Cells (iPSCs) for the development of new models of cardiac tissues, new disease models and drug screening. Interest in iPSCs models has increased due to the clinical need for *in vitro* tissue models to mimic the complexity of cardiac tissue and create new therapies for CVD [3]. These iPSCs models can overcome the limitations of adult cell models [4] and give rise to iPSC-CMs [5]. Although these models are promising, they also have limitations, since the substrates where iPSC-CMs are cultivated do not allow maturation and functionality representative of a mature and adult heart, which hinders the development of reliable and relevant therapies for CVD [6–8].

In order to overcome these limitations, this project aims to bioengineer a culture substrate that combines ECM components (gelatin) that will be functionalized with conductive materials, specifically LIG. LIG is obtained by laser irradiating suitable carbon-based precursors by photoconverting $sp^3$ carbon atoms into $sp^2$ carbon atoms, resulting in a three-dimensional structure of highly conductive porous graphene. Electrical functionalization by incorporating conductive materials such as LIG into the substrate will serve to

stimulate immature iPSC-CMs and enhance cardiac tissue maturation by combining the biocompatibility and bioactivity of the ECM with the conductivity and anisotropy of the LIG. H. T. H. Au et al. emphasized that the combination of mechanical, anisotropic, and electrical characteristics is essential for creating functional cardiac tissue [9]. This will allow the development of more biologically representative cardiac models similar to the adult human myocardium.

Recently, graphene has also been described as a biocompatible conductive material that can be used to electrically stimulate cells [10]. However, the standardized production of graphene has some disadvantages, such as the long manufacturing time and the need for high processing temperatures combined with the use of expensive and toxic chemicals, which significantly hinder the wide application of this material [11]. On the other hand, LIG production is achievable with computer-controlled laser systems, resulting in a one-step, maskless, scalable and cost-effective approach for graphene fabrication with tunable morphology, porosity and composition [12] on the desired substrates. In addition, LIG is more environmentally friendly, flexible, and mechanically robust than graphene, and it also boasts excellent electrical and thermal properties [13]. These factors led to the consideration of LIG for this work. The synthesis of LIG on various substrates such as Polyimide (PI) [14], textiles, wood and cellulose [15] has already been reported in various studies. It has also been employed in various applications, from strain sensors [14] to energy storage devices [16] and biosensors [15, 17, 18]. There are no reports of LIG production using gelatin-only that can promote maturation of iPSC-CMs [19, 20].

Although it has never been reported, the appealing features of LIG and gelatin created the hypothesis that gelatin/LIG platforms could be a versatile mean to stimulate maturation. Furthermore, the aim is to generate highly conductive anisotropic topographies using this technology [21]. By allowing for the generation of combined anisotropy and conductivity of the maturation of iPSC-CMs, tissue-specific anisotropy and tissue biological function can be achieved.

Results were obtained proving the successful role of native cardiac ECM in promoting the maturation of iPSC-CMs [19]. In addition, several biomaterials, both natural and synthetic, have been used to mimic the cardiac biological environment. Such natural biomaterials include: collagen, fibrin, fibronectin, matrigel and decellularized ECM, whereas the synthetic ones include: Polycaprolactone (PCL), Polylactic Acid (PLA) and Polyethylene Glycol (PEG) [22].

In this project, gelatin was the biomaterial designed to mimic the ECM of the natural heart, thereby creating a biologically suitable environment for cells.

In summary, the substrate consisting of gelatin will be functionalized with LIG, not only allowing for the combination of the properties of gelatin and LIG but also, opening new perspectives for applications in the area of Tissue Engineering (TE). The choice of gelatin is driven by their cost advantage over pure collagen, enabling their broader use in all conducted tests.

The objectives of the study include: (i) the determination of the formulation of the

biomaterial (focusing on the proportion between the non-cytotoxic materials used and the mechanical properties of the films produced), (ii) the definition of the adequate conditions for the efficient formation of LIG and (iii) to carry out cellular assays.

The research work described in this dissertation was carried out in accordance with the norms established in the ethics code of Universidade Nova de Lisboa. The work described and the material presented in this dissertation, with the exceptions clearly indicated, constitute original work carried out by the author.

# 2

# State of the art

The adult human heart has an extremely limited capacity for regeneration, with an estimated renewal rate of CMs of 1% per year, which decreases with advancing age [23], posing a significant challenge in the context of cardiac pathologies. There is evidence pointing to an epidemic increase in heart failure, with one of the causes being the reduction in the number of CMs. This reduction in CMs can occur as a result of a cardiac event, such as a heart attack, or due to degenerative processes over time, which can affect heart function and contribute to the progression of heart failure. Therefore, current therapies focus on preserving the remaining CMs but face the intrinsic challenge of regenerating the lost CMs.

According to the review by Z. Lin and W. T. Pu, there are currently different strategies under investigation to regenerate the myocardium, such as: (i) inducing existing CMs in the heart to re-enter the cell cycle; (ii) delivering *ex vivo* isolated and expanded Cardiac Progenitor Cells (CPCs) or their derivatives to the heart; (iii) enhancing the activity of endogenous CPCs; and (iv) directly reprogramming non-CMs into CMs [24]. The authors demonstrated the ability to induce the generation of new CMs by stimulating existing CMs with growth factors, causing them to re-enter the cell cycle, and observed their mechanical, electrical, and vascular integration in the myocardium. However, this procedure may present oncogenic potential, so it is crucial to evaluate this approach before applying it in a clinical setting - strategy (i) [24]. Additionally, researchers also addressed cell therapy as one of the approaches used for this problem. This approach involves the transplantation of different types of cells for cardiac regeneration. To mitigate the risk of arrhythmia associated with trials using this approach, more recent studies have utilized cardiomyogenic activity progenitor cells or their differentiated derivatives. These cells have been derived from pluripotent stem cells such as Embryonic Stem Cells (ESCs) or iPSCs, as well as from adult progenitor cells present in the heart (resident CPCs or non-resident CPCs located in non-cardiac areas). Injection of CMs derived from human ESCs resulted in stable grafts that improved cardiac function in rats with myocardial infarction [25]. However, in addition to important ethical considerations, there are challenges and limitations to be considered, such as the relative immaturity of these ESCs-derived CMs,

the need for immunosuppression to prevent graft rejection, and the safety and longevity of grafts. The objective of this therapy is to isolate, amplify, differentiate, and then transplant progenitor cells or their descendants - strategy (ii) [24]. An alternative strategy is to enhance the regenerative activity of resident CPCs. Data indicates that CPCs do not substantially differentiate into CMs during normal homeostasis. However, myocardial injuries stimulate increased generation of CMs from non-myocardial cells - strategy (iii). As a result, there are multiple cardiac regeneration strategies in development, each with its own advantages and challenges [24]. With a focus on the cell therapy strategy (ii), C. Fischer et al. demonstrated that adult cardiac tissue can be maintained under electromechanical stimuli, although some alterations at the structural, mechanical, and gene expression levels are detected [26]. Nevertheless, an approach to tackle this challenge is presented in the study conducted by H. V. Almeida et al., where it was demonstrated the potential of human cardiac ECM on the phenotype and maturation characteristics of iPSC-CMs. It was shown that human cardiac ECM can be decellularized, isolated, fragmented, and successfully incorporated into three-dimensional iPSC-CMs aggregates, promoting phenotypic, structural, and ultrastructural maturation of CMs, further enhancing calcium handling. High cell viability and metabolic activity were observed over a period of 20 days. Thus, this strategy offers a solution for cardiac microenvironment regulation, paving the way for advances in cell therapy, drug screening, and disease modeling [20].

Although biochemical approaches have shown great potential in the context of cardiac regeneration, there are still some challenges to overcome. In this sense, TE emerges as an alternative to tackle these challenges and seek innovative solutions, with CTE standing out. CTE aims to develop structures that mimic the characteristics of the myocardial ECM, with the goal of promoting cardiac tissue development [27].

CMs undergo changes in their cytoskeleton and morphology when exposed to different substrates. Therefore, when producing these substrates, it is crucial to consider certain characteristics such as ease of fabrication, miniaturization, flexibility, and the ability to maintain CMs contractility, ideally without external electrical stimulation [28].

In literature, there are several studies investigating the impact of scaffolds/substrates on cellular behaviour. P. J. Gouveia et al. demonstrated that the use of scaffolds promoting alignment of CMs results in better tissue cohesion, and scaffolds enhancing electrical signal propagation among CMs exhibit high levels of proteins associated with muscle contraction. Additionally, the application of external electrical fields to scaffolds seeded with CMs has been shown to induce a higher rate of tissue maturation [28]. The study by J. Wang et al. expressed the beneficial use of flexible and conductive substrates in the maturation and development of CMs. It posited that a graphene substrate, as a conductive biomimetic surface, could facilitate intrinsic electrical propagation, mimicking the microenvironment of the native heart, to further promote the global maturation of Human Induced Pluripotent Stem Cell-Derived Cardiomyocytes (hiPSC-CMs) [10].

Within the field of CTE, biomaterials play a crucial role in influencing cell activity,

adhesion, proliferation, maturation, and differentiation. Nanotechnology has been essential in enhancing engineered cardiac tissues, allowing for the optimization of substrate properties for specific applications. Small differences in nanostructure can have impacts on the macro-scale and tissue function. The ideal biomaterial for CTE needs to possess suitable properties such as the ability to support efficient attachment, growth, and differentiation of CMs, resulting in the formation of functional cardiac tissue [29].

In CTE, natural and synthetic biomaterials have been used. Among natural biomaterials, collagen, fibrin, fibronectin, matrigel and decellularized ECM stand out [22, 29]. Among synthetic biomaterials, the following have been used: PCL, PLA and PEG [22, 30]. As mentioned earlier, the focus of this study will be collagen-based biomaterials and their derivatives, such as gelatin, aiming to generate LIG. Gelatin exhibits intriguing properties, and its combination with conductive materials may enhance its performance in cellular stimulation.

Recently, conductive materials like graphene have also been used for TE applications due to their unique mechanical, thermal, optical, and electrical properties, as well as their biocompatibility. The study conducted by J. Wang et al. also demonstrated that graphene can be used to enhance electrical stimulation of CMs and promote their differentiation [10]. Although standard graphene production offers various advantages, it also has some disadvantages, such as high production costs, long fabrication time, and the need for high processing temperatures combined with the use of expensive and toxic chemicals. In this regard, LIG overcomes these limitations, and its discovery from polymers in 2014 has garnered significant attention in recent years [13]. The laser induces localized temperature increases, leading to selective graphitization and a shift from the native hybridization of the carbons into precursor materials to $sp^2$ hybridization in graphene structures. The LIG synthesis method enables efficient and cost-effective conversion of a polymer substrate into LIG [31]. This results in an excellent alternative to conventional graphene with adjustable morphology, porosity, and composition. Additionally, LIG utilizes scalable and roll-to-roll compatible methods which jointly with its low toxicity, flexibility, robustness and excellent mechanical and electrical properties make LIG a promising candidate to use in TE applications. Another interesting advantage is the ability to generate LIG from a wide range of carbon precursors using multiple lasers, such as infrared, ultraviolet, and visible ranges. The study conducted by T. Pinheiro et al. also highlighted that different operating parameters, such as Power and Speed, resulted in different laser penetration depths and different properties of the final LIG films. Therefore, careful optimization of these parameters is crucial [15]. The aromatic composition of the precursor material also plays a significant role in the properties of the films produced by laser irradiation/exposure. Additionally, the use of inert gases such as Argon (Ar) has shown to be beneficial in increasing the efficiency of LIG production compared to environments with oxygen presence. Table 2.1 presents certain substrates that have been used as substrates for the production of LIG, as well as the applications of the produced LIG films [31]. Materials such as: PI, Polydimethylsiloxane (PDMS),

chitosan, gelatin, chromatographic paper and office paper were considered to be used with different applications.

Table 2.1: Representation of different precursor materials capable of generating LIG and their respective applications and objectives as substrates.

| Substrates | Description | Applications and Objectives | Bibliographic References |
|---|---|---|---|
| PI | LIG electrodes produced on PI substrates, connected to PDMS microchannels. | Microfluidic electrochemical biosensor integrated with LIG for the diagnosis of CVD. | [32] |
| PI and PDMS | Heart rate sensors utilizing graphene-based detection elements in conjunction with the HeartPy toolkit for Python. 1° - LIG produced on PI substrates. 2° - LIG produced on PI substrates with PDMS coating. | Low-cost and easily accessible sensor for beginner developers of heart rate sensors enabling experimentation and widespread application. | [33] |
| PI and chitosan--Glucose Oxidade (GOx) | Approaches tested with different materials: 1° - Flexible LIG electrodes produced on PI substrates. 2° - Flexible LIG electrodes produced on PI substrates, where the chitosan-GOx composite was immobilized on their surface. | Flexible, low-cost, rapid, and selective electrochemical biosensor for glucose detection. | [34] |

| Materials | Description | Applications and Objectives | Bibliographic References |
|---|---|---|---|
| PI and gelatin | PI film coated with gelatin. Gelatin absorbed the intense laser impact and helped adjust the surface morphology. | Microsupercapacitors were fabricated using the prepared LIG revealing enormous potential for flexible electronics. | [35] |
| Chitosan | Production of LIG from chitosan biopolymers. | Production of flexible films from a new class of sustainable marine materials - chitosan biopolymers. | [36] |
| Chromato--graphic and office paper (cellulosic materials) | Production of LIG from paper with proper chemical treatment. | Development of films electrochemical systems based on LIG for enzymatic glucose sensors on paper, increasing sustainability, accessibility, and reducing costs. | [15] |

During film production, it is crucial to use agents to promote the crosslinking of collagen or its derivatives. Without these agents, the films exhibit reduced stability and mechanical properties in aqueous environments, which can result in their disintegration over time. A study conducted by M.G. Haugh et al. investigated the effects of the Dehydrothermal Treatment (DHT) on Collagen-Glycosaminoglycan (CG) scaffolds, where increased temperature and duration of the treatment resulted in improved mechanical properties of the scaffolds. It was concluded that DHT is a viable technique to enhance the mechanical properties of CG scaffolds, making them more suitable for *in vitro* and *in vivo* use [37]. Similar to DHT, genipin is also used as a crosslinking agent. In a study conducted by H.G. Sundararaghavan et al., the effect of genipin treatment concentration and the duration on the mechanical properties of type I collagen gels were investigated. It was observed that genipin promotes crosslinking, thereby imparting stiffness to type I collagen gels, which influences cellular behaviour. Thus, genipin is a useful agent for modulating the mechanical properties and cellular behaviour in collagen gels [38].

Therefore, when developing the biomaterial, the choice of the crosslinking agent is a crucial step. Moreover, the inclusion of a fire-retardant in the films composition is

essential to give them higher termal resistance, i.e. a fire-retardant allows expanding the range of laser operating conditions, which is benefecial for evaluating the best properties for LIG formation [15]. To address the notable thermal degradation and ablation typically witnessed when such substrates undergo laser irradiation, chemical treatments involving specific retardants have been proposed. Notably, retardants based on phosphate [39, 40] and boric derivatives such as boric acid [40] and sodium tetraborate (Borax)[41] have been utilized. Specifically, boric-based inorganic metal hydrates, like borax, have been intensively explored to mitigate thermal degradation of natural fibers, such as cellulose [42], while concurrently serving as thermal dissipaters during laser-induced combustion, owing to their endothermic decomposition processes that can prevent substrate ignition [43].

# 3

# Materials and Methods

This chapter presents the experimental methodologies employed in the production and subsequent characterization of the films developed throughout this project, as well as the evaluation of their cell viability. Two distinct groups were tested: (a) containing gelatin (CAS: 9000-70-8) and sodium tetraborate decahydrate ($Na_2B_4O_7{\cdot}10H_2O$; ≥99.5%; CAS: 1303-96-4) and (b) composed of gelatin (CAS: 9000-70-8), genipin ($C_{11}H_{14}O_5$; ≥98%; CAS: 6902-77-8) and sodium tetraborate decahydrate ($Na_2B_4O_7{\cdot}10H_2O$; ≥99.5%; CAS: 1303-96-4). Gelatin was sourced from Merck, while sodium tetraborate decahydrate and genipin were obtained from Sigma-Aldrich.

In approach (a), the crosslinking was achieved using DHT. According to this method, increased temperatures allow for the formation of a denser and more robust polymeric structure [44]. On the other hand, in approach (b), genipin was used, a chemical crosslinking agent, which is responsible for forming covalent bonds between the polymeric chains [38]. The main objective of the application of these 2 types of crosslinking agents is to improve the physical and chemical characteristics of the gelatin films. Other crosslinking technique was adopted during the swelling and degradation tests, the substrates that underwent the crosslinking approaches (a) and (b) began to disintegrate upon contact with the Phosphate-buffered saline (PBS) solution and the LIG quickly dissolved.

## 3.1 Biomaterial formulation and optimized conditions for LIG generation

### 3.1.1 Film Formulation

#### 3.1.1.1 Film composed of Gelatin and Sodium Tetraborate Decahydrate

Firstly, a solution was prepared using water as solvent, with 10% (w/v) gelatin, maintaining the temperature at 45 ºC. After one hour, a concentration of 1.91% (w/v) sodium tetraborate decahydrate was added to the solution [15]. After 30 minutes, the temperature was reduced to 25 ºC. The procedure is presented in Figure 3.1.

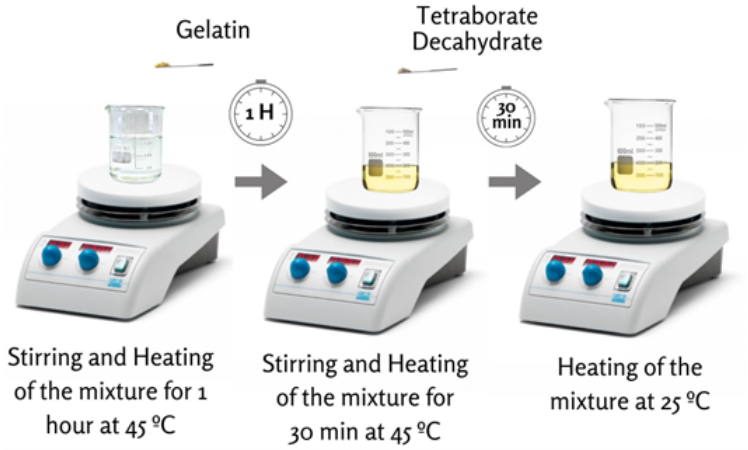


Figure 3.1: Schematic representation of the production of Gel-NaB films.

#### 3.1.1.2 Film composed of Gelatin, Genipin and Sodium Tetraborate Decahydrate

The procedure stated in section 3.1.1.1 was followed to produce the gelatin and sodium tetraborate decahydrate solution.

A concentration of 0.0022% (w/v) of genipin was added to the solution, which was then stirred for 3 hours. The color change of the solution from yellow to a bluish-green shade indicated the occurrence of crosslinking [45]. The procedure is presented in Figure 3.2.

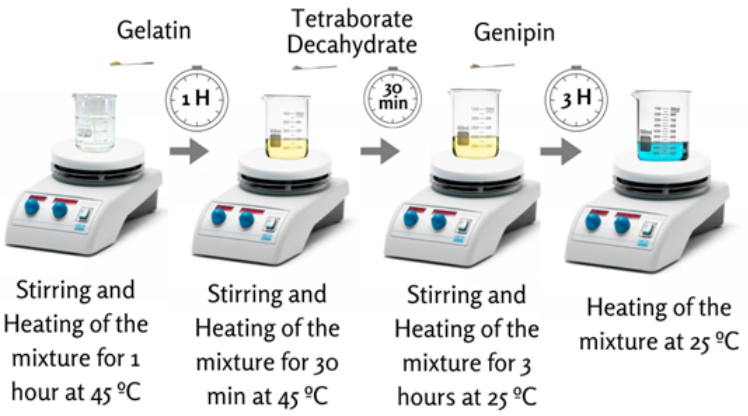


Figure 3.2: Schematic representation of the production of Gel-Gen-NaB films.

### 3.1.2 Film Deposition and Drying Method

Subsequently, molds were produced to deposit the solutions. The acetate material was placed on a glass substrate to facilitate the removal of the film after drying.

The gelatin and sodium tetraborate decahydrate solution was casted in the mold, which was placed on a heating plate with an initial temperature of 25 ºC. The temperature was gradually increased by 5 ºC every 30 minutes until reaching 45 ºC [46]. This procedure is defined as Dehydrothermal Treatment (DHT) and aims to promote a slow

drying of the film and prevent bubble formation. The film was then left to dry overnight, approximately for 12 hours.

The solution composed of gelatin, genipin and sodium tetraborate decahydrate was casted in the mold which was then placed on a heating plate at 25 ºC. This temperature was maintained constant throughout the night to ensure stable conditions during the process. The procedure is presented in Figure 3.3.

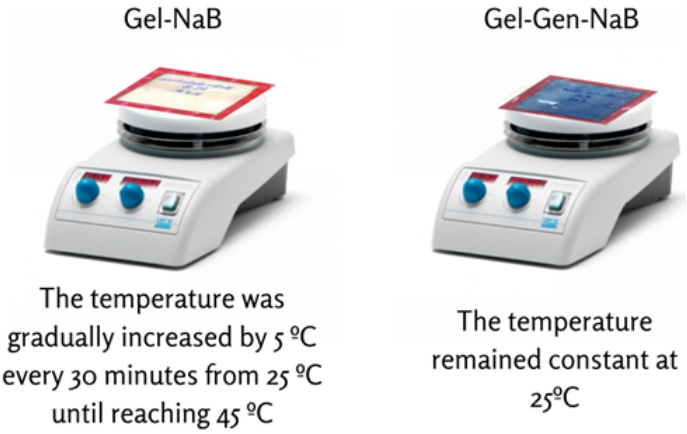


Figure 3.3: Schematic representation of the drying method.

As previously mentioned, the films began to disintegrate upon contact with the Phosphate-buffered saline (PBS) solution. To enhance their resistance, they were immersed in an 1-Ethyl-3-(3-dimethylaminopropyl)carbodiimide-N-Hydroxysuccinimide (EDC-NHS) solution, aiming to stabilize the substrate against degradation in aqueous environments. Despite the toxicity of this chemical crosslinking agent for cells, it was considered appropriate [47] since a strategy was developed to neutralize its harmful effects by submersing it in a PBS solution [47], in order to mitigate any harmful impact on the cells.

### 3.1.3 Crosslinking treatment with EDC-NHS

Two solutions of EDC and NHS with concentrations of 5% and 2.5%, respectively, were prepared [48].

The Gel-NaB and Gel-Gen-NaB films were immersed in the EDC-NHS solution for 2 hours and then left to dry overnight. The following day, these films were immersed in a PBS solution, and left to dry again overnight.

Subsequently, the films underwent laser exposure, where several laser power, scan speed, Pulses per Inch (PPI), Z-axis position, image density and image enhancement were tested.

### 3.1.4 Optimized Conditions for LIG Generation

Laser-Induced Graphene (LIG) was produced using a computer-controlled $CO_2$ laser

cutting machine (VLS 3.50, Universal Laser Systems), with a 10.6 $\mu$m wavelength, a pulsed cutting laser associated with a 2.0 type plano-convex lens and 50W power [49]. The vector image software *Adobe Illustrator* (Adobe Systems, Ireland) was used to draw the adopted geometry: a 7 mm x 7 mm square, which is a suitable size for cell culture. During all the experiments, nitrogen flow and exhaust were continuously on.

#### 3.1.4.1 Film prior to immersion in EDC-NHS and PBS solutions

Both films, composed of: (a) gelatin and sodium tetraborate decahydrate (Gel-NaB) and (b) gelatin, genipin, and sodium tetraborate decahydrate (Gel-Gen-NaB), prior to immersion in 1-Ethyl-3-(3-dimethylaminopropyl)carbodiimide (EDC)-N-Hydroxysuccinimide (NHS) and PBS solutions, were subjected to the laser parameters described in Table 3.1.

Table 3.1: Optimized values for the laser variables: Power, Speed, PPI, Z-axis Position, Image Density and Image Enhancement of the mentioned films (prior to immersion in EDC-NHS and PBS solutions).

| Power [W] | Speed [m/s] | PPI | Z-axis Position | Image Density | Image Enhancement |
|---|---|---|---|---|---|
| 0.25 | 0.2032 | 1000 | 0.300″ | 7 | Auto: No Margin |

The Power corresponds to the amount of energy emitted by the laser during its operation. The Speed refers to how quickly the laser moves across the material. PPI represent the number of laser pulses applied per inch. The Z variable describes the separation between the laser lens and the surface of the material. Image Density quantifies the number of dots etched by the laser in each square inch, while Image Enhancement adjusts the processing of the image by the laser.

#### 3.1.4.2 Film after immersion in EDC-NHS and PBS solutions

Both films, composed of: (a) gelatin and sodium tetraborate decahydrate (Gel-NaB-EDC) and (b) gelatin, genipin, and sodium tetraborate decahydrate (Gel-Gen-NaB-EDC), after immersion in EDC-NHS and PBS solutions, were subjected to laser exposure, according to the parameters stated in Table 3.2.

Table 3.2: Optimized values for the laser variables: Power, Speed, PPI, Z-axis Position, Image Density and Image Enhancement of the mentioned films (after immersion in EDC-NHS and PBS solutions).

| Power [W] | Speed [m/s] | PPI | Z-axis Position | Image Density | Image Enhancement |
|---|---|---|---|---|---|
| 1 | 0.2286 | 1000 | 0.300″ | 7 | Auto: No Margin |

After the LIG production, a 0.05% (w/v) gelatin solution was deposited to ensure LIG consistency during all experiments. Before carrying out the cell culture, the samples were sterilized through a 20-minute bath in a 70% ethanol solution, followed by immersion under UV light.

## 3.2 Characterization

### 3.2.1 Micro-Raman Spectroscopy

Raman spectroscopy is a technique that assesses the quality of graphene, providing details about the electronic structure and atomic vibrations in the material. It allows the identification of defects, impurities and the number of graphene layers by analyzing three main peaks in Raman spectra: G, D, and 2D. The G peak is related to the vibration of carbon atoms in graphene. The D peak reflects defects and impurities in graphene, its presence being minimal in high-quality samples. The 2D peak is a second order of the D peak, being fundamental for the determination of the number of graphene layers. The equipment used for the analysis was the Renishaw in Via Qontor Raman Microscope [50]. The wavelength of the laser used was 532 nm. A 1200 l/mm grating was used. The acquisition time was 10 seconds and 3 accumulations were performed.

### 3.2.2 Four-Point Probe Resistivity Measurement Device

The equipment used to measure the sheet resistance of the material was the Biorad HL5500 Hall Effect systems using the four-point probe method or Van der Pauw method, which assumes homogeneity, isotropy, and uniformity of the sample thickness [51]. After determining the sheet resistance of the film [Ω/sq], it was possible to calculate the electrical conductivity of the material [S/m] through the following equation 3.1:

$$\sigma = \frac{1}{\rho} = \frac{1}{R_{\text{sh}} \cdot t} \tag{3.1}$$

, where $\sigma$ corresponds to conductivity [S/m], $\rho$ corresponds to resistivity [Ω·m], $R_{sh}$ corresponds to the sheet resistance of the material [Ω/sq], and t corresponds to the thickness of LIG [m]. The thickness of the LIG was determined through the Scanning Electron Microscopy (SEM) technique.

### 3.2.3 SEM

SEM is a technique that provides information on the morphology and topography of a substrate surface [52]. The equipment used for this analysis was the Hitachi TM3030 Plus Tabletop microscope [53] and due to the need for electrical conduction in this technique, the samples were coated with 20 nm Iridium (Ir) layer [54]. In addition, SEM was used to measure the thickness of the LIG, allowing for the conductivity to be calculated from

the sheet resistance, as mentioned earlier. The porosity of the LIG produced was also obtained from the analysis of SEM images using *Fiji* software.

### 3.2.4 Optical Stereo Microscope

Leica M80 Optical Stereo Microscope was used to study the surface morphology of the samples [55].

### 3.2.5 Cellular Assays

Cell culture was performed at NOVA Medical School using undifferentiated single Human Induced Pluripotent Stem Cells (hiPSCs), which were expanded in Essential 8 Medium in a 12-well plate. Differentiation was initiated by replacing the medium in each well with 1.5 mL of RPMI, supplemented with B27 serum without insulin (GibcoTM), 12 $\mu$M CHIR, 100 ng/mL Activin A, and 270 $\mu$M of Ascorbic Acid, to induce Cardiomyocytes (CMs) differentiation. The procedure done along the culture period followed a previously published protocol [56].

#### 3.2.5.1 Live/Dead Staining

Cell viability and their morphological changes were assessed on days 1, 3, and 6 using an Invitrogen viability/toxicity kit from Thermo Fisher Scientific. 2 $\mu$L of ethidium homodimer-1 and 0.5 $\mu$L of calcein AM were added to 0.5 mL of PBS solution per well as described in the manufacturer's protocol. Images of the cells were captured using a Carl Zeiss Microscopy GmbH microscope, 15 minutes after performing the viability assay and analysed using *ImageJ* software. First, all cells were counted, and then the percentage of viable cells was calculated, compared to a control group where the viability is 100%. To calculate cell size, the aforementioned software was also used. Statistical analyses, using *GraphPad Prism* software, were performed and data were expressed as mean ± Standard Deviation (SD). A one-way ANOVA, followed by Tukey's post hoc test, was utilized for identifying significant group differences.

#### 3.2.5.2 Presto Blue Assay

Cell proliferation was assessed with the $PrestoBlue^{TM}$ Assay (Invitrogen), using the Invitrogen's $PrestoBlue^{TM}$ Cell Viability Reagent from Thermo Fisher Scientific. In a 1:10 concentration, as per the manufacturer's protocol, the reagent was added to each well, followed by a 30-minute incubation. Then, 100 $\mu$L in duplicates was withdrawn from each well to a 96-well plate. This plate was then placed in a SpectraMax i3x Multi-Mode Microplate Reader for fluorescence evaluation, through *SoftMax Pro* software. The results were then compared with those of a control group. This assay was performed on days 1, 3, and 6, on 5 samples of each group.

#### 3.2.5.3 Immunofluorescence Staining

The immunofluorescence protocol begins with the fixation of the cells, followed by washing the samples in a PBS bath for 30 minutes, and then permeabilization in 0.1% Triton X-100 (Sigma-Aldrich) for 30 minutes. The samples are then incubated in a blocking solution with 2% Bovine serum albumin (BSA) (Sigma-Aldrich) for 30 minutes to prevent nonspecific binding. Subsequently, they are incubated with the primary antibody, Monoclonal Anti-$\alpha$-Actinin (Sigma-Aldrich), diluted in a blocking solution at 1:800, overnight. After three 5-minute washes in PBS, the secondary antibody, Goat anti-Mouse IgG, Alexa Fluor™ 488 (Thermo Fisher Scientific), diluted at 1:500 in the blocking solution, which ended up being applied to the samples and incubated for 1 hour. After a one-hour wash in PBS, the cells are treated with 4',6-Diamidino-2-phenylindole (DAPI) diluted in PBS at 1:100 for nuclear staining, during 15 minutes. Finally, the samples are washed three times in PBS, each wash lasting 5 minutes, before the visualization under the Carl Zeiss Microscopy microscope.

#### 3.2.5.4 SEM

The samples were immersed in baths of 50, 70, 80, 90, and 100% ethanol for 5 minutes each, respectively. The samples were then coated with a 20 nm Gold(Au)/Palladium(Pd) conductive layer and analyzed using SEM to evaluate the presence of cells.

# 4

# Results and Discussion

In this chapter, the results of the experimental methodologies used to characterize the films developed and the LIG produced in them are presented. Additionally, the assessment of cell viability on substrates is discussed. As previously mentioned, two distinct groups were tested: (a) one containing gelatin and sodium tetraborate decahydrate and (b) another composed of gelatin, genipin and sodium tetraborate decahydrate. The results of film characterizations before and after immersion in EDC-NHS and PBS solutions will be presented.

## 4.1 Characterization of films

### 4.1.1 Film prior to immersion in EDC-NHS and PBS solutions

Regarding the properties of the Gel-NaB film, it is important to mention that it has a yellow color, also being translucent and brittle, while the Gel-Gen-NaB film has a blue color, is slightly less translucent and exhibits a lower susceptibility to breaking, which can be seen in Figure 4.1.

(a) Gel-NaB film.

(b) Gel-Gen-NaB film.

Figure 4.1: Comparison between the films produced. Scale bar corresponds to 1 cm.

The fact that the Gel-NaB film is more brittle may be associated to the DHT that occurred, in which the gradual increase in the film's drying temperature led to the evaporation of water molecules, decreasing the mechanical integrity of the film.

It should be noted that during film production it is crucial to minimize the presence of bubbles in the solution, as these bubbles can influence LIG production, impacting the characteristics of the film.

The optimization of the laser processing parameters was carried out in parallel with the development of the film formulation. After producing several films and carrying out optimizations in the laser process, the ideal parameters were achieved for the variables Power, Speed, PPI, Z-axis Position, Image Density and Image Enhancement. These values are detailed in Table 3.1 of Chapter 3.1.4.1 of Materials and Methods. Image Density values below 7 compromised the desired standard and, as such, this value was adopted. It is concluded that, for the substrates in question, it is preferable to use a higher vertical resolution, that is, a greater number of pixel lines per vertical inch, producing more accurate vector details [57].

As the film produced is not entirely homogeneous, variations in the laser effect occur, resulting in the synthesis of LIG with variable characteristics throughout the sample, which can be seen in Figure 4.2. Consequently, there is intra-sample variation in the chemical properties of the LIG generated.

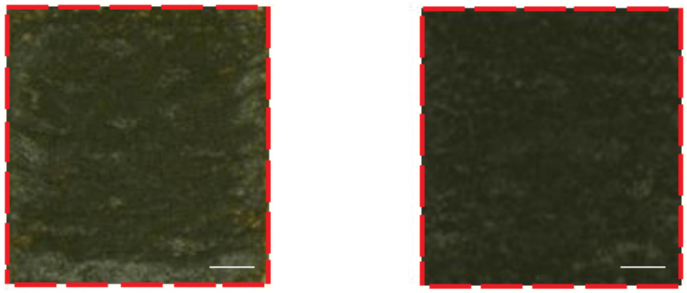

(a) Gel-NaB film. (b) Gel-Gen-NaB film.

Figure 4.2: Images of the LIG produced from the substrates. Scale bar corresponds to 1 mm.

The morphology of the LIG generated in the developed film was carried out using the SEM technique. The purpose was to investigate how the same laser operating conditions influence the topography of the film surface. The results are presented in Figure 4.3.

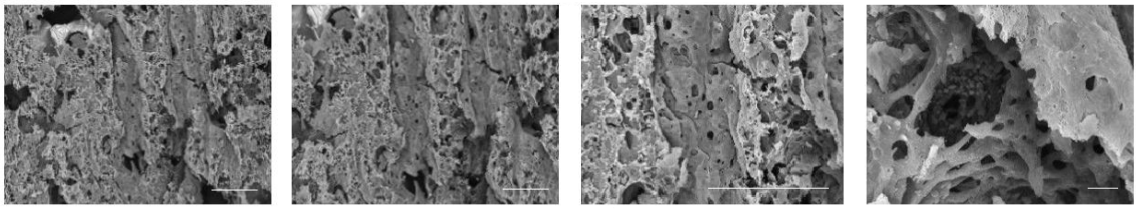

(a) Gel-NaB film.

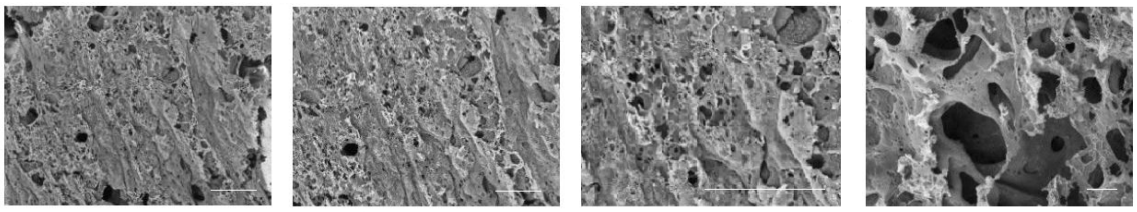

(b) Gel-Gen-NaB film.

Figure 4.3: SEM analysis of the films produced. Scale bar corresponds to 200 $\mu$m, except for the $4^{th}$ column of images, where it corresponds to 10 $\mu$m.

The analysis of both films revealed different morphological features. The Gel-NaB film had a higher porosity of (56 ± 2) % compared to the Gel-Gen-NaB film, which had a porosity of (52 ± 3) %. The presence of marks resulting from the laser action on the films is noticeable, presenting the formation of "channels". The porosity was determined using the image volume method, which involves summing up the porosity pixels from all analyzed images and then dividing this total by the sum of the areas observed in these images. This resulting value is then multiplied by 100%.

A cross-section analysis was also carried out in three squares of each group with LIG generated, with the aim of converting the sheet resistance ($R_{sh}$) [Ω/sq] obtained by the Hall Effect into conductivity [S/m]. It can be seen in Figure 4.4 the SEM images of the generated film and LIG.

Using *ImageJ* software, the thickness of the films was determined. The Gel-NaB film had a thickness of (270 ± 200) $\mu$m, while that of LIG was (330 ± 200) $\mu$m. In turn, the Gel-Gen-NaB film recorded a thickness of (280 ± 80) $\mu$m and the LIG of (300 ± 80) $\mu$m. It is observed that the thickness of the two films are very similar. However, the thickness of the LIG is consistently higher in both cases, which would be expected. This is due to the process induced by the laser that converts the material into LIG, resulting in multiple layers and, consequently, an increase in the total thickness of the material.

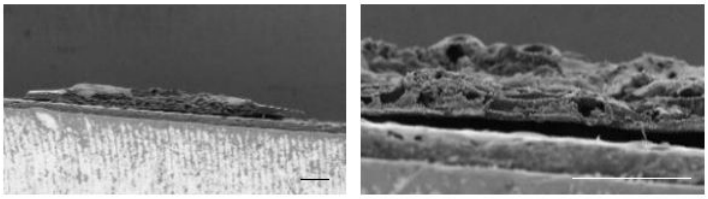

(a) Gel-NaB film.

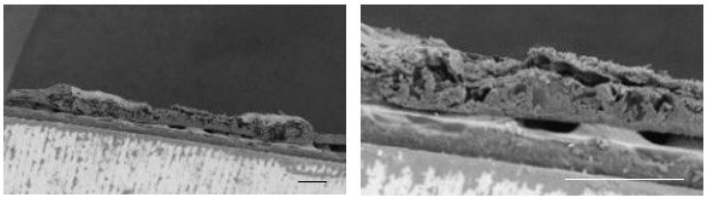

(b) Gel-Gen-NaB film.

Figure 4.4: SEM analysis to determine the thickness of the LIG and film produced. Scale bar corresponds to 500 $\mu$m. n=3.

Raman spectroscopy was used to study and identify the presence of LIG in the sample. Three distinct peaks are generally identified in the Raman spectrum: the D, G and 2D peak. Peak D, located at approximately 1350 $cm^{-1}$ in the Raman spectrum, is a crucial indicator of the presence of defects or disorders in carbon-based materials. This peak is characteristic of materials containing $sp^2$-hybridized carbon atoms, which form a flat hexagonal network typical of graphene and other forms of carbon. However, unlike the G peak, which reflects the presence and quality of $sp^2$ carbon, the D peak arises specifically due to the perturbation of this perfect hexagonal lattice. The presence and intensity of peak D are directly proportional to the degree of disorder or imperfection in the material. This may include point defects or other irregularities in the hexagonal structure. In a perfect graphene crystal, for example, peak D would be absent, since there would be no disorder or defects to cause its formation. The appearance of this peak is a consequence of first-order inelastic processes that only occur when there are defects in the material. The relationship between the intensities of peaks D and G is used to evaluate the quality of the material, whereas a higher I(D)/I(G) ratio indicates a greater amount of disorder or defects. Peak G is found around 1580 $cm^{-1}$ and, as previously mentioned, its presence serves as an indicator of the presence of $sp^2$ carbon structures, typical of graphene and graphite. Therefore, the G peak is the result of first-order inelastic processes and is associated with the stretching vibration in the plane of the bonds of $sp^2$ carbon atoms. The 2D peak, also called the G' peak, is found at around 2700 $cm^{-1}$ and is the result of a second-order inelastic dispersion process. In monolayer graphene, the 2D peak is particularly notable because it appears as a single, well-defined, high-intensity peak, contrasting with graphite, where it is possible to observe multiple 2D components. The presence and shape of this peak are indicatives of the number of graphene layers present in the sample as well as possible tensions or deformations in the material. For example,

a I(2D)/I(G) intensity ratio that is significantly greater than one typically indicates the presence of a monolayer graphene [15].

The substrates which were analyzed and the spectra are shown in Figure 4.5.

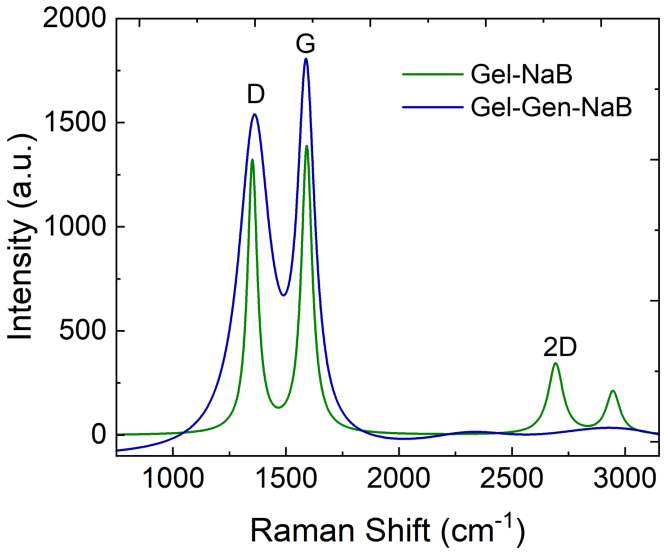


Figure 4.5: Raman spectra of the LIG produced in the films of Gel-NaB and Gel-Gen-NaB. n=3.

Three distinct peaks were identified in the Raman spectrum of the Gel-NaB film, located around (1349 ± 5), (1592 ± 5) and (2690 ± 50) $cm^{-1}$, and correspond to the D, G and 2D peaks characteristic of carbon-based structures [58]. In the Gel-Gen-NaB film, only two well-defined peaks were recognized, located approximately at (1363 ± 4) and (1587 ± 3) $cm^{-1}$. These values coincide with peaks D and G, mentioned above. In the Table 4.1 the ratios between the intensities of peaks D and G and 2D and G are represented.

Table 4.1: Chemical properties obtained by Raman spectroscopy and electrical properties of LIG produced from the substrates of Gel-NaB and Gel-Gen-NaB. n=3. Results presented as mean ± standard error.

| Substrate | I(D)/I(G) | I(2D)/I(G) | $R_{sh}$ [Ω/sq] | $t_{LIG}$ [$\mu$m] | $\sigma$[S/m] |
|---|---|---|---|---|---|
| Gel-NaB | 0.95 ± 0.05 | 0.3 ± 0.2 | 292 ± 20 | 330 ± 200 | 14 ± 9 |
| Gel-Gen-NaB | 0.85 ± 0.03 | 0.02 ± 0.01 | 162 ± 50 | 300 ± 80 | 23 ± 3 |

The I(D)/I(G) ratio showed that the Gel-NaB film presents a slight predominance of disorder, with a ratio of 0.95 ± 0.05, compared to the Gel-Gen-NaB film which registered 0.85 ± 0.03. This result suggests that the former has a greater amount of disorder or defects in its $sp^2$ carbon structure. In contrast, analysis of the I(2D)/I(G) ratio revealed more pronounced differences. The Gel-NaB film showed a ratio of 0.3 ± 0.2, while the Gel-Gen-NaB film registered a very low value of 0.02 ± 0.01, signaling a potential presence

of multiple layers of graphene or a structure that comes closer to that of graphite (it should be considered that to calculate the ratio between the intensities of the 2D and G peaks, for the Gel-Gen-NaB film (where the 2D peak is less pronounced), it was assumed that the intensity around (2904 ± 60) $cm^{-1}$ represented that of the 2D peak). These results, obtained under identical laser conditions, emphasize the fundamental influence that the substrate has in determining the quality and structure of the generated LIG. In conclusion, the LIG of the Gel-NaB film revealed itself to be more disordered, but closer to a structure with fewer layers compared to that of the Gel-Gen-NaB film, with the latter then revealing itself to be a multilayered and more ordered structure.

In regards to the electrical and conductive properties of the LIG, the sheet resistance ($R_{sh}$) [Ω/sq] and conductivity ($\sigma$) [S/m] values are also represented in Table 4.1. When evaluating the resistivity of materials, it is important to consider some limitations due to the porous characteristics of the LIG produced from the substrates, which can be seen from the SEM images in Figure 4.3.

In Table 4.2, a literature review is presented focusing on the chemical and electrical properties of LIG produced from different substrates. The objective is the comparison the obtained results with the characteristics reported in the literature for LIG derived from different polymeric materials.

Table 4.2: Comparison of the chemical properties obtained by Raman spectroscopy and electrical properties of LIG produced from different substrates.

| Substrate | I(D)/I(G) | I(2D)/I(G) | $R_{sh}$ | Ref. |
|---|---|---|---|---|
| Gel-Gen-NaB | 0.85 | 0.02 | 162 | - |
| Polyimide (PI) | 0.44 | 0.88 | 15 | [12] |
| PI | 0.60 | 0.60 | n.a. | [59] |
| PI | <1 | >0.2 | 85 | [60] |
| Polyetherimide (PEI) | 0.20 | 0.65 | 84 | [40] |
| PI/Polydimethylsiloxane (PDMS) | 0.72 | 0.61 | 80 | [61] |
| Kraft lignin/poly(ethylene oxide) (KL/PEO) | 0.50 | 0.40 | 363 | [62] |

It is concluded that the LIG generated on PI [60], Gel-NaB and Gel-Gen-NaB substrates presents greater disorder compared to the other substrates listed in Table 4.2. The LIG generated on the Gel-Gen-NaB substrate stands out for being the closest to the graphite structure in terms of multilayers. On the other hand, the PEI material stands out for its highly ordered structure, which suggests that this substrate is a potential candidate

to produce high-quality graphene. The impact of genipin on the structure of Gel-Gen-NaB is notable, bringing it closer to graphite. In future studies, it could be interesting to investigate the impact of different concentrations of genipin on the final structure.

Regarding the conductive properties of materials, sheet resistance is an important metric that measures the electrical resistance of a material, and, generally, materials with lower sheet resistance have better electrical conductivity. Among the substrates analyzed, Gel-Gen-NaB stands out for presenting a significantly lower sheet resistance, $(162 \pm 50)\ \Omega/\text{sq}$, compared to Gel-NaB, $(292 \pm 20)\ \Omega/\text{sq}$. Furthermore, Gel-Gen-NaB also demonstrates superior electrical conductivity when compared to Gel-NaB. This difference indicates that the addition of genipin contributes positively to electrical conductivity. Furthermore, when analyzing the ratios between peak intensities, it is observed that the Gel-Gen-NaB substrate is closer to the graphite structure. This suggests that a structure closer to graphite may have benefits in terms of electrical conductivity. On the other hand, the PI substrate [12] not only presents the lowest sheet resistance - signaling the best conductivity among the listed materials - but also, I(D)/I(G) and I(2D)/I(G) values that suggest a structure closer to graphene. This may reinforce the potential relationship between the material's structure and its electrical conductivity. In contrast, the KL/PEO substrate, which exhibited the highest sheet resistance, had an intermediate I(D)/I(G) ratio.

While only sheet resistance values are provided, it's key to understand that conductivity is intrinsically tied to the thickness of the LIG on the material. This means that a material, even with a higher sheet resistance, can exhibit high conductivity if the LIG is sufficiently thin. Typically, materials are compared based on their conductivity and the intensity ratio between peaks. However, given the available data, the comparison was primarily based on sheet resistance values and intensity ratios.

### 4.1.2 Film after immersion in EDC-NHS and PBS solutions

Regarding the properties of the films after immersion in the EDC-NHS solution, it was observed that they presented a slightly more pleated structure after drying since the EDC-NHS solution is often used to promote crosslinking in biological polymers. When films are immersed in this solution, it is possible for film molecules to react and form crosslinks. This reaction alters the original structure of the films and, upon drying, these new bonds can cause localized contractions in the polymer matrix, resulting in the pleated appearance observed.

After preparing the film for laser processing, the previously used parameters were applied. However, due to the different chemical characteristics of these films, it became evident that these parameters did not produce the desired LIG pattern. Thus, it was concluded that it was essential to evaluate the laser processing conditions adequate to produce LIG in the newly prepared films.

Therefore, optimization of the parameters for the films in question was undertaken.

Initially, operation was conducted with a power of 0.25 W (0.5%) and a speed of 0.2032 m/s (16%). After optimization, adjustments were made to a power of 1 W (2%) and a speed of 0.2286 m/s (18%). Although the changes were not very significant, they were crucial to achieving the desired standard and obtaining LIG with visibly satisfactory characteristics, which can be seen in Figure 4.6.

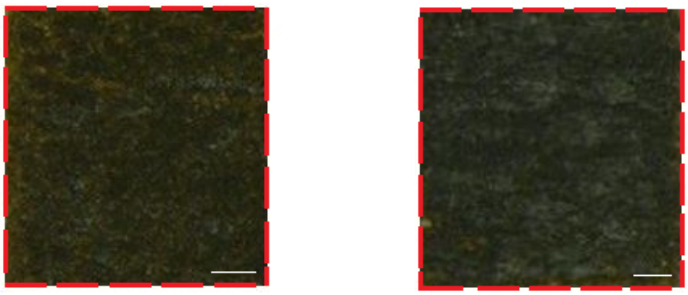

(a) Gel-NaB-EDC film.

(b) Gel-Gen-NaB-EDC film.

Figure 4.6: Images of the LIG produced from the substrates. Scale bar corresponds to 1 mm.

The PPI, Z-axis position, Image Density, and Image Enhancement values were kept constant. During the optimization process, power and speed values were adjusted. Power ranged from 0.1% (equivalent to 0.05W) to 5% (equivalent to 2.5W), and speed varied from 5% (0.0636m/s) to 25% (0.3175m/s). The selected values aimed to closely match the electrical conductivity of cardiac tissue, which ranges from 0.16 S/m longitudinally to 0.005 S/m transversely [63]. These values are detailed in Table 3.2 of Chapter 3.1.4.2 from the Materials and Methods section.

When analyzing the morphology of LIG in the films, it was observed that, after the immersion in the EDC-NHS solution, it presented a higher porosity than those not subjected to the immersion process. Specifically, the Gel-NaB-EDC film has a porosity of (66 ± 4) %, while the Gel-Gen-NaB-EDC film has an even higher porosity of (70 ± 2) %. The marks from the laser action appear less pronounced on the films that underwent immersion, which can be seen in Figure 4.7. Among the immersed films, the Gel-Gen-NaB-EDC film displays a more irregular structure compared to the Gel-NaB-EDC film, leading to a less defined pattern.

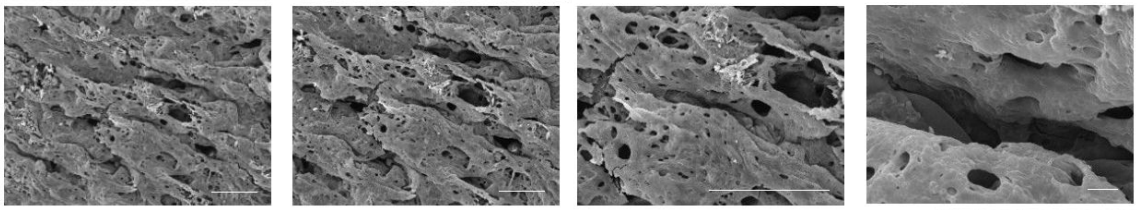

(a) Gel-NaB-EDC film.

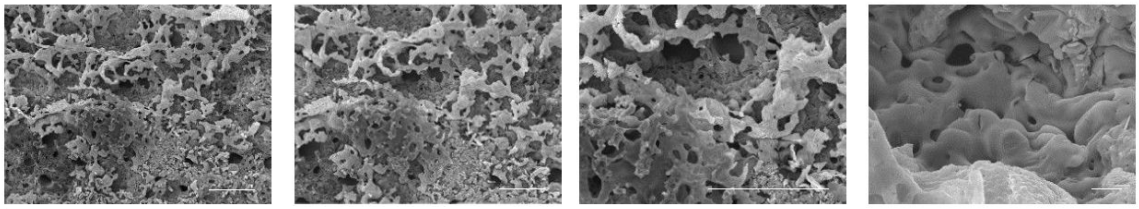

(b) Gel-Gen-NaB-EDC film.

Figure 4.7: SEM analysis of the films produced. Scale bar corresponds to 200 $\mu$m, except for the $4^{th}$ column of images, where it corresponds to 10 $\mu$m.

The thickness of the films was evaluated. The Gel-NaB-EDC film had a thickness of (140 ± 20) $\mu$m, while its LIG was (170 ± 30) $\mu$m. On the other hand, the Gel-Gen-NaB-EDC film had a thickness of (170 ± 30) $\mu$m and its LIG was (240 ± 40) $\mu$m. In both cases, the thickness of the LIG was greater than that of the original film. It is notable that the increase in LIG thickness was more pronounced in the Gel-Gen-NaB-EDC film than in the Gel-NaB-EDC film, which can be seen in Figure 4.8. A potential reason for this could be that genipin enhances the laser energy absorption or influences a distinct heat distribution during the laser process, leading to a thicker LIG layer.

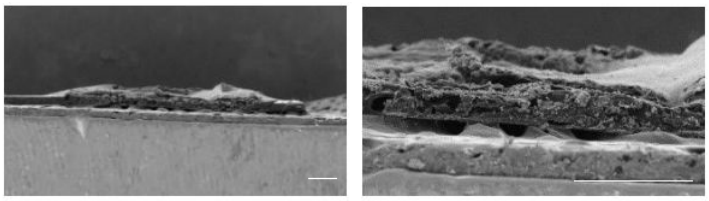

(a) Gel-NaB-EDC film.

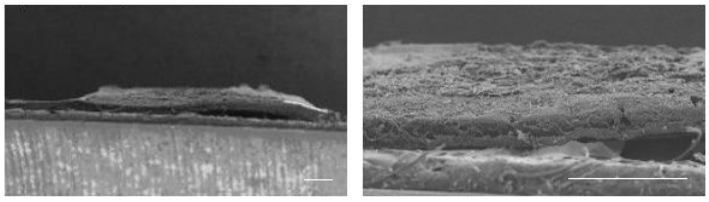

(b) Gel-Gen-NaB-EDC film.

Figure 4.8: SEM analysis to determine the thickness of the LIG and film produced. Scale bar corresponds to 500 $\mu$m. n=3.

When comparing the thickness before and after immersion in the EDC-NHS solution, it is observed that it decreases after immersion. A possible explanation for this is the action of the EDC-NHS solution, which may have promoted the formation of crosslinks between the film molecules, making the matrix more compact. This compaction can result in a decrease in overall thickness. Furthermore, the EDC-NHS solution may have removed or solubilized less-bound or non-crosslinked components of the film, contributing to the thinner thickness after immersion.

The substrates were analyzed using Raman spectroscopy, and the spectra are shown in Figure 4.9.

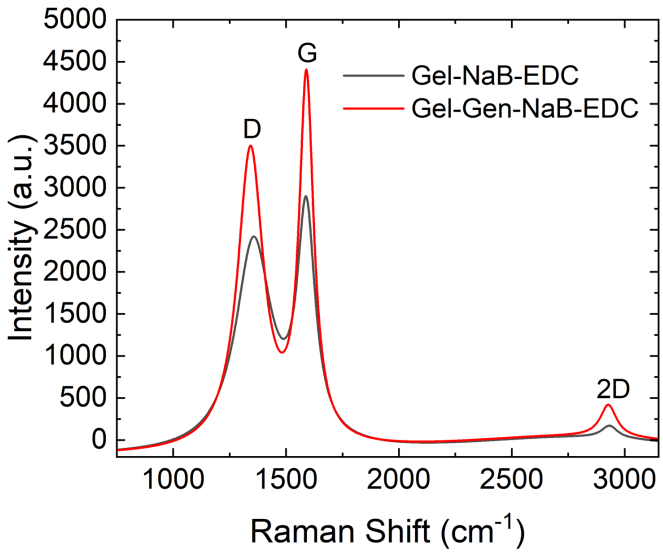


Figure 4.9: Raman spectra of LIG produced in films of Gel-NaB-EDC and Gel-Gen-NaB-EDC. n=3.

Three distinct peaks were identified in the Raman spectrum of the Gel-NaB-EDC film, located around (1358 ± 8), (1587 ± 5) and (2932 ± 50) $cm^{-1}$, which correspond to the D, G and 2D peaks characteristic of carbon-based structures. In the spectrum of the Gel-Gen-NaB-EDC film the peaks are located approximately at (1345 ± 10), (1587 ± 6) and (2927 ± 40) $cm^{-1}$. When comparing with the spectra of other substrates, it is observed that the 2D peaks of these two films are further from the reference value, 2700 $cm^{-1}$. This displacement may be indicative of changes in the order and alignment of the carbon planes in the films. The ratios between the intensities of peaks D and G, as well as 2D and G, are represented in Table 4.3.

Table 4.3: Chemical properties obtained by Raman spectroscopy and electrical properties of the LIG produced from the substrates of Gel-NaB-EDC and Gel-Gen-NaB-EDC. n=3. Results presented as mean ± standard error.

| Substrate | I(D)/I(G) | I(2D)/I(G) | $R_{sh}$ [Ω/sq] | $t_{LIG}$ [$\mu$m] | $\sigma$[S/m] |
|---|---|---|---|---|---|
| Gel-NaB-EDC | 0.84 ± 0.04 | 0.06 ± 0.01 | 1530 ± 30 | 170 ± 30 | 4.0 ± 0.7 |
| Gel-Gen-NaB-EDC | 0.79 ± 0.02 | 0.09 ± 0.02 | 5730 ± 30 | 240 ± 40 | 0.8 ± 0.2 |

The Gel-NaB-EDC film exhibits a I(D)/I(G) ratio of 0.84 ± 0.04, indicating that, like the Gel-NaB film (with a I(D)/I(G) ratio of 0.95 ± 0.05), there is a significant amount of disorder or defects in its $sp^2$ carbon structure. However, this value is slightly lower than that of the film without EDC-NHS, suggesting that the introduction of EDC-NHS may have promoted better ordering of its structure. On the other hand, the Gel-Gen-NaB-EDC film has a I(D)/I(G) ratio of 0.79 ± 0.02, lower than its counterpart without EDC-NHS (with 0.85 ± 0.03). This lower value suggests a slightly more ordered structure, possibly due to EDC-NHS, which may favor more stable crosslinks. Regarding the I(2D)/I(G) ratio, Gel-NaB-EDC presents a value of 0.06 ± 0.01, lower than that of the film without EDC-NHS (0.3 ± 0.2). This decrease suggests that the presence of EDC-NHS may have led to a more layered structure. The Gel-Gen-NaB-EDC film has a I(2D)/I(G) ratio of 0.09 ± 0.02, higher than that of the film without EDC-NHS (0.02 ± 0.01), reinforcing the idea that EDC-NHS can affect the formation of multilayers.

In conclusion, EDC-NHS appears to influence the ordering and multilayer structure of LIG in films. Both Gel-NaB-EDC and Gel-Gen-NaB-EDC films, when treated with EDC-NHS, show a more ordered structure than their counterparts without EDC-NHS, as revealed by the I(D)/I(G) ratio. However, when evaluating the number of layers, measured by the I(2D)/I(G) ratio, it becomes clear that EDC-NHS does not have a uniform effect: while in Gel-NaB-EDC, EDC-NHS seems to favor the formation of more layers, while in Gel-Gen-NaB-EDC the effect is the opposite. This highlights the importance of considering the specific interaction between film type and EDC-NHS, reflecting the inherent complexity in modulating LIG properties based on the reagents and preparation methods used.

Regarding the electrical properties of LIG, the $R_{sh}$ (Ω/sq) and conductivity ($\sigma$) (S/m) values are represented in Table 4.3. Among the films analyzed, Gel-NaB-EDC has a sheet resistance of (1530 ± 30) Ω/sq. This value is lower than that recorded for the Gel-Gen-NaB-EDC film, which is (5730 ± 30) Ω/sq. This distinction suggests that, although the presence of genipin, in the context without EDC-NHS, improved conductivity (as observed in previous results), when combined with EDC-NHS, it appears to increase sheet resistance and, consequently, reduce electrical conductivity of the material. Therefore, the combination of genipin and EDC-NHS may not be the most suitable for optimizing

electrical conductivity.

Regarding the ratios between the peak intensities of the films with EDC-NHS, differences are observed in their characteristics. The Gel-NaB-EDC film, despite having lower sheet resistance and, consequently, greater conductivity, reveals I(D)/I(G) and I(2D)/I(G) ratios which suggest a more disordered structure. On the other hand, Gel-Gen-NaB-EDC, with its higher sheet resistance, appears to have a less graphite-like structure, as inferred from the I(2D)/I(G) ratio. This analysis illustrates that, even though peak ratios provide information about the structure of the material, other factors, possibly related to the combination of genipin and EDC-NHS, play a crucial role in the electrical properties. In conclusion, the Gel-NaB-EDC film, although showing a more disordered structure, has a higher electrical conductivity. In contrast, Gel-Gen-NaB-EDC, even with a slightly more organized structure, does not exhibit such outstanding electrical properties.

When comparing the conductivity values, with and without EDC-NHS, it is evident that the Gel-Gen-NaB-EDC film is closer to the typical conductivity values of natural cardiac tissue, which ranges from 0.16 S/m longitudinally to 0.005 S/m transversely [63].

### 4.1.3 Challenges faced during the film development process

During the film development process, several challenges arose, mainly in determining the appropriate concentrations of gelatin and NaB, as well as the apropriate drying method. Different concentrations of gelatin, such as 5, 10, and 25% (w/v), were tested. At a concentration of 5% (w/v), problems emerged in the production of LIG due to an insufficient concentration of gelatin. Increasing to 25% (w/v), the film became quite thick, with a texture similar to rubber, which can be seen in Figure 4.10. After the laser processing step, the generated square displayed a brownish hue and a powdery residue was formed, causing the material to disintegrate. Finally, when using a concentration of 10% (w/v), it was possible to produce robust and homogeneous LIG.

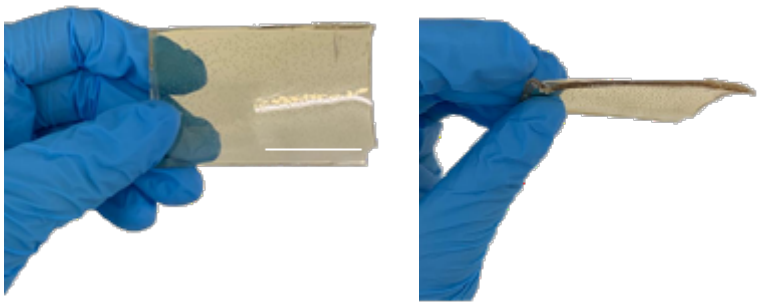

(a) (b)

Figure 4.10: Gel-NaB film with a concentration of 25% (w/v) gelatin. Scale bar corresponds to 3 cm.

Two different concentrations of NaB: 1.91 and 3.82% (w/v), were also tested. The concentration of 3.82% (w/v) was initially chosen based on previous studies carried

out on paper [15]. With this concentration, after the film dried, sodium tetraborate decahydrate crystals appeared, preventing the formation of LIG, which can be seen in Figure 4.11. Consequently, it became evident that this concentration was too high. Thus, the NaB concentration was halved, which allowed for adequate LIG production.

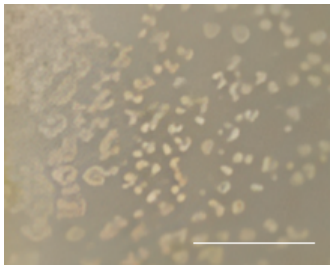

Figure 4.11: Gel-NaB film with a concentration of 3.82% (w/v) NaB. Scale bar corresponds to 1.5 cm.

As for the drying process, different methods were explored, such as the oven and the heating plate. In the oven, during the DHT of one of the films, the temperature was increased by 5 ºC every 10 minutes, from 25 ºC to 140 ºC over a period of 12 hours. However, visible cracks were observed in the film after the drying step, which can be seen in Figure 4.12. On the heating plate, when the temperature was slowly increased to approximately 80 ºC, the film also became fragile and very brittle. Therefore, it was determined that the best drying approach would be to use the heating plate at a lower temperature. In the specific case of the Gel-NaB film, the ideal was to gradually increase the temperature by 5 ºC every 30 minutes, until reaching 45 ºC.

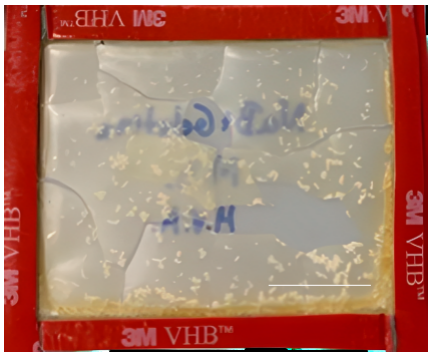


Figure 4.12: Gel-NaB film subjected to DHT, with a gradual increase in temperature of 5 ºC every 10 minutes, from 25 ºC to 140 ºC.

## 4.2 Cellular assays

### 4.2.1 Cells Viability and Morphology Assessment

The films used as substrates for cell culture were: Gel-NaB-EDC and Gel-Gen-NaB-EDC. The viability of Induced Pluripotent Stem Cell-Derived Cardiomyocytes (iPSC-CMs) was qualitatively assessed using the Live/Dead assay on days 1, 3 and 6, as shown in Figure 4.13. Due to the intense fluorescence signal of the substrates, especially in the red region, it was not possible to observe dead cells. Therefore, the decision was made to draw comparisons based on a graph representing the total area of living cells.

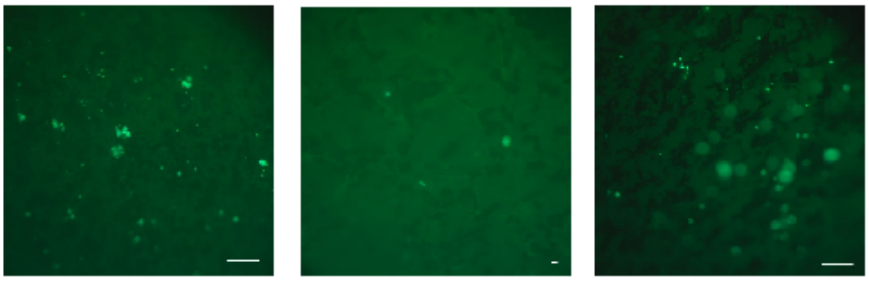

(a) Gel-NaB-EDC film. Days 1, 3 and 6, respectively.

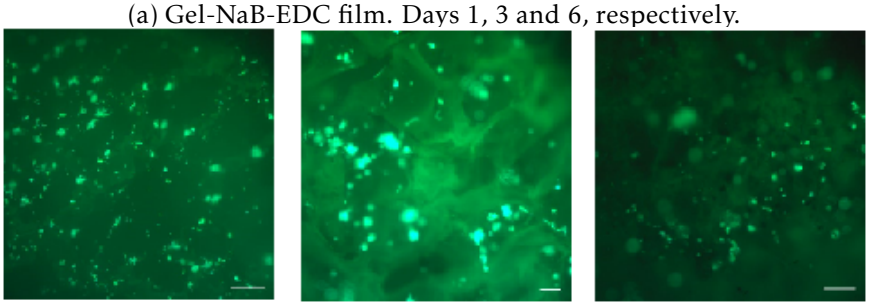

(b) Gel-Gen-NaB-EDC film. Days 1, 3 and 6, respectively.

Figure 4.13: Representative image of the Live/Dead Assay for the films. Scale bar corresponds to 20 $\mu$m.

As illustrated in Figure 4.14, the Gel-NaB-EDC film exhibited variable behavior over time. Initially, a drastic reduction in live cells was observed between days 1 and 3, followed by a significant increase until day 6. On the other hand, the Gel-Gen-NaB-EDC film showed a more stable trend of decrease in living cells. On the first day, the film with genipin showed a much higher total area of living cells compared to the film without genipin, indicating that it may be more biocompatible or efficient in promoting initial cell adhesion.

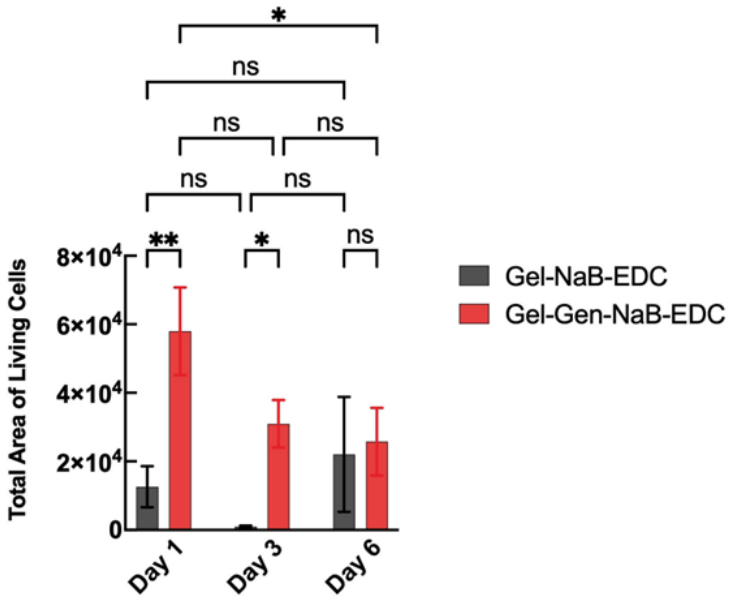


Figure 4.14: Graph representing the Total Area of Living Cells at 3 different timepoints. n=3. Throughout, data are presented as mean ± SD *p < 0.05, **p < 0.01, ***p < 0.001, ****p < 0.0001, ns, not significant, determined by one-way ANOVA followed by Tukey's HSD test (*GraphPad* Software).

Although the cells show good proliferation, it is essential to take cellular morphology into account. After 6 days of culture, the cells on the Gel-NaB-EDC film still have a rounded shape and not the elongated morphology expected from differentiated iPSC-CMs, which can be seen in Figure 4.15.

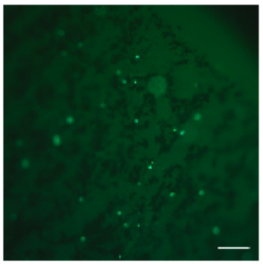

(a) Gel-NaB-EDC film. Day 6.

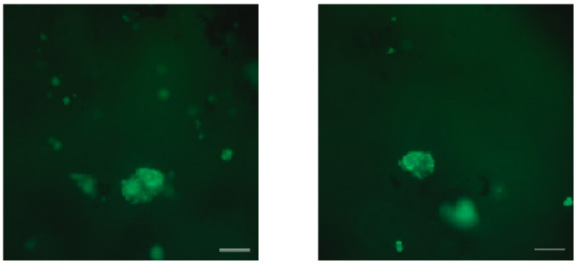

(b) Gel-Gen-NaB-EDC film. Day 6.

Figure 4.15: Morphometric analysis of the films on the sixth day of the Live/Dead Assay. Scale bar corresponds to 20 $\mu$m.

Like other cell types, iPSC-CMs react to the rigidity of the substrate they come into contact with. As a result of this interaction, they form a large protein complex called focal adhesions, which connects the cellular cytoskeleton to the matrix. On softer substrates, it is often observed the formation of a greater number of focal adhesions but of smaller dimensions. These do not disperse widely throughout the matrix, resulting in a more rounded cell morphology [64]. Therefore, it is clear that the stiffness of the substrate directly influences the morphology and function of iPSC-CMs. Substrates with an ideal stiffness can promote the maturation and adequate sarcomeric organization of iPSC-CMs in culture. The observed behavior of the cells in the film is probably a consequence of its low rigidity. Cellular morphology is a crucial indicator of the phenotype and differentiation level of iPSC-CMs, as it reflects specific gene expression and cell differentiation profiles. It should be noted that, unlike many other cells, adult CMs have a limited capacity for proliferation and a highly organized structure with sarcomeres. The stiffness response may affect this sarcomeric organization.

Thus, the cells encapsulated in the Gel-NaB-EDC film do not show signs of contractile phenotypic differentiation after 6 days due to their rounded morphology. On the other hand, those encapsulated in the Gel-Gen-NaB-EDC film have a more developed morphology, reflecting the possible influence of film rigidity on the differentiation of iPSC-CMs.

When analyzing images of cells in culture, it is crucial to consider the Average Size, which represents the average size of the cells. The Average Size is calculated from the average of the areas of all particles identified in the image and can provide information about cellular behavior, such as proliferation, grouping and differentiation, which can be seen in Figure 4.16.

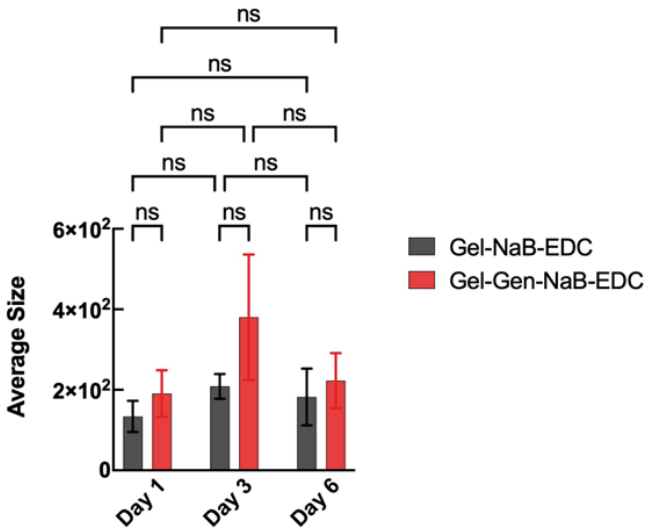


Figure 4.16: Average Size of iPSC-CMs at 3 different timepoints. n=3. Throughout, data are presented as mean ± SD *p < 0.05, **p < 0.01, ***p < 0.001, ****p < 0.0001, ns, not significant, determined by one-way ANOVA followed by Tukey's HSD test (*GraphPad* Software).

In the Gel-NaB-EDC film, an initial increase in the average cell size is observed, followed by a reduction. However, the average size on the sixth day still exceeds that on the first day, which indicates possible cell growth or clustering over time. On the other hand, in the Gel-Gen-NaB-EDC film, the average cell size increases notably on the third day, then reduces on the sixth day, although it remains higher than on the first day. This pattern suggests that the cells may be proliferating or clustering intensely at first, then stabilizing.

Throughout the study period, the Gel-Gen-NaB-EDC film presented, on average, larger cells, when compared to the Gel-NaB-EDC. This indicates that the properties of the film with genipin might be more favorable to cellular behavior, resulting in an increase in cell size.

In conclusion, the results indicate that both substrates influence the differentiation and maturation of iPSC-CMs, as evidenced by the observed increase in cell size. Notably, the Gel-Gen-NaB-EDC film presented a better performance in terms of biocompatibility and promotion of differentiation of iPSC-CMs in the long term. This is corroborated by the more notable presence of live cells, as well as the increase in their average size during the study. Cell morphology on the Gel-Gen-NaB-EDC film also suggests that the rigidity of this substrate exerts a greater influence on the differentiation of iPSC-CMs, a vital characteristic for cardiac functionality. Therefore, in contexts such as Cardiac Tissue Engineering (CTE), the Gel-Gen-NaB-EDC film may be the most suitable option.

### 4.2.2 Metabolic Activity

The metabolic activity of the cultures, assessed by the $PrestoBlue^{TM}$ assay after 1, 3 and 6 days of culture, is shown in Figure 4.17.

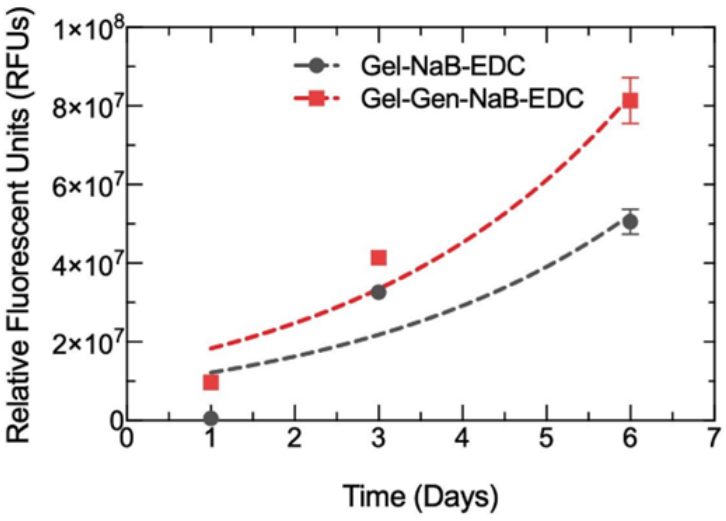


Figure 4.17: Graph of $PrestoBlue^{TM}$ assay results for days 1, 3 and 6. Exponential adjustment. n=3.

At the beginning of the culture (Day 1), the cells of the Gel-Gen-NaB-EDC film showed

a significantly higher Relative Fluorescent Units (RFUs) value than those of the Gel-NaB-EDC film, suggesting greater cell viability or proliferation in the genipin film. Although cells in both films showed an increase in RFUs over time, those in the genipin film maintained higher values, thereby standing out in promoting the desired cellular behavior.

From the exponential adjustment of the curve presented in Figure 4.17, the doubling time was calculated for each group, as indicated in Table 4.4. These values were obtained from the exponential curve fit.

Table 4.4: Exponential adjustment value equivalent to the growth rate and cell doubling time for each group. n=3.

| Substrate | Growth Ratio | Doubling Time (Days) |
|---|---|---|
| Gel-NaB-EDC | 0.29 | 2.38 |
| Gel-Gen-NaB-EDC | 0.30 | 2.30 |

In the Gel-NaB-EDC film, the Growth Ratio is 0.29, and the Doubling Time, is 2.38 days. On the other hand, the Gel-Gen-NaB-EDC film has a slightly higher Growth Ratio of 0.30 and a slightly shorter Doubling Time of 2.30 days. This difference, although subtle, suggests that the cells in the film with genipin (Gel-Gen-NaB-EDC) proliferate a little more quickly, managing to double their population in a shorter period. Thus, for Tissue Engineering (TE) applications, the Gel-Gen-NaB-EDC film appears to be a more promising option, contributing to creating a more favorable environment for cell proliferation.

### 4.2.3 Immunofluorescence Staining

Immunofluorescence makes it possible to visualize specific proteins in cellular samples. Alpha Actinin ($\alpha$-Actinin), highlighted in green, is a muscle cytoskeleton protein expressed in CMs. Their location in the Z lines of sarcomeres indicates the organization of the heart's contractile fibers, and their presence and organization are indicative of the maturation and functionality of these CMs. On the other hand, DAPI, when binding to DNA, identifies cell nuclei with a blue color [65].

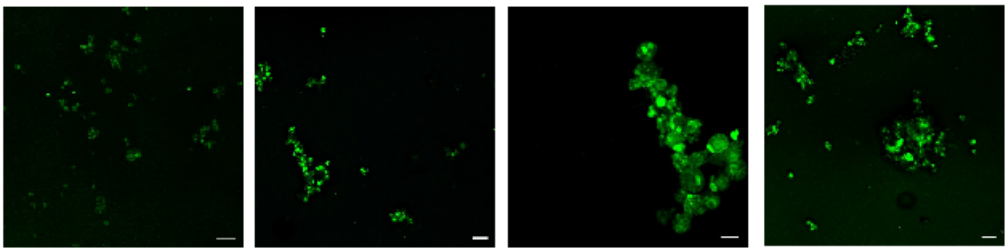

(a) Gel-NaB-EDC film.

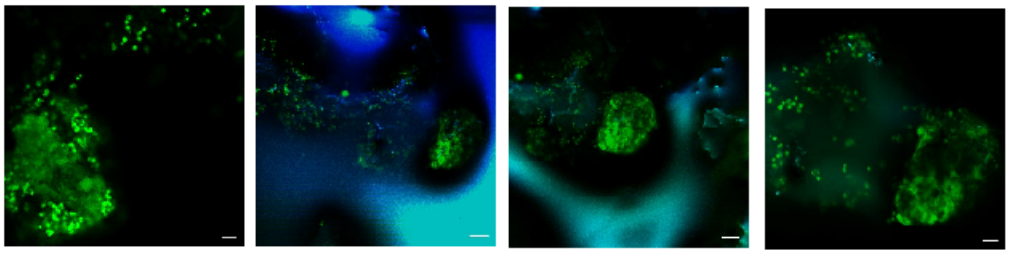

(b) Gel-Gen-NaB-EDC film.

Figure 4.18: Representative image of Immunofluorescence on the $6^{th}$ day of cell culture for the films. Scale bar corresponds to 20 $\mu$m.

When evaluating the fluorescence intensity on the sixth day, it was noticed that the Gel-NaB-EDC film presented green aggregates characteristic of $\alpha$-Actinin. The organization and density of these aggregates reflect the degree of maturation of the iPSC-CMs, as the most mature tend to exhibit a more defined sarcomeric structure. However, the disposition of these aggregates in the Gel-NaB-EDC film differs from that observed in the Gel-Gen-NaB-EDC film, suggesting that in the latter, the iPSC-CMs present more cohesive and advanced sarcomeric structures. The absence of blue coloration was observed in the Gel-NaB-EDC film, indicating limited visualization of cell nuclei. In contrast, in the Gel-Gen-NaB-EDC film, cell nuclei are clearly visible, indicating cell viability. Combining these observations with the data on cell proliferation already discussed, the proposal is reinforced that the Gel-Gen-NaB-EDC film offers a more favorable environment for the development and maturation of iPSC-CMs.

### 4.2.4 SEM

When observing the SEM images of the Gel-NaB-EDC and Gel-Gen-NaB-EDC films seeded with cells, it is important to highlight that human adult CMs generally have lengths of the order of 100 $\mu$m and widths between 10-30 $\mu$m [66]. When analyzing the images, structures that stood out and presented circular shapes, typical of these cells, were sought.

However, a significant difference was observed between the two samples. In the Gel-Gen-NaB-EDC film, there was a greater number of more prominent circular structures. These, due to their dimensions, could indicate mature iPSC-CMs or clusters of these cells.

This observation suggests that the substrate Gel-Gen-NaB-EDC may promote the development of more mature iPSC-CMs or the formation of denser clusters, when compared to Gel-NaB-EDC.

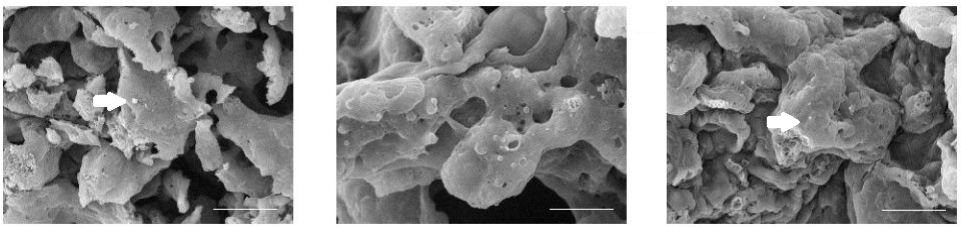

(a) Gel-NaB-EDC film. Days 1, 3 and 6, respectively.

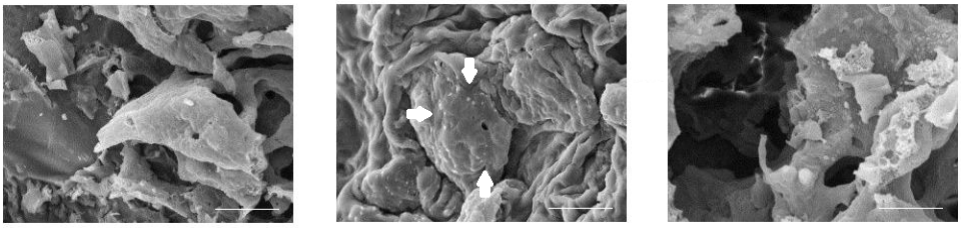

(b) Gel-Gen-NaB-EDC film. Days 1, 3 and 6, respectively.

Figure 4.19: SEM images of days 1, 3 and 6 of cell culture of the films. Scale bar corresponds to 20 $\mu$m.

Therefore, and considering all the cellular characterizations carried out, it is clear that the film with genipin stood out in promoting ideal conditions for the growth and differentiation of iPSC-CMs. Cell viability on the genipin film was significantly better, indicating its greater compatibility with iPSC-CMs. Regarding morphology, the iPSC-CMs cultured on this film exhibited more defined contours, aligning more with the typical morphology of mature CMs. At the same time, the film with genipin promoted greater cell proliferation over time, highlighting its role as a favorable environment for the maturation of iPSC-CMs. Regarding cellular structuring, organization and density of $\alpha$-Actinin aggregates were more evident in the film with genipin and a clearer visualization of cell nuclei was also observed, highlighting the presence and potential maturation of iPSC-CMs.

Taking these characteristics into account, there is no doubt that the genipin film would be the substrate of choice for the next stage of electrical stimulation of iPSC-CMs.

# 5

# Conclusions and Future Perspectives

The growing prevalence of Cardiovascular Diseases (CVD), recognized as the leading cause of global death, highlights the importance of developing innovative therapeutic alternatives in the treatment of cardiac pathologies [1]. CTE has stood out as a promising area in this context. However, one of the main challenges lies in the maturation and functionality of iPSC-CMs in physiological contexts. The appropriate selection of biomaterials is crucial, given that many conventional substrates cannot induce cellular maturation to mimic the functionality of an adult human heart [29].

Considering the importance of integrating mechanical, anisotropic, and electrical properties in creating functional cardiac tissues, this study focused on bioengineering, a culture substrate that mimics natural cardiac Extracellular Matrix (ECM). This substrate combines components of the ECM, such as gelatin, with conductive materials, namely LIG. Particularly, the influence of the substrates Gel-NaB-EDC and Gel-Gen-NaB-EDC on the proliferation, differentiation, and maturation of iPSC-CMs was investigated.

During the characterization of the films, Gel-NaB and Gel-Gen-NaB, both before and after immersion in the EDC-NHS solution, significant differences were observed in terms of color, transparency, and fragility. After optimizing the films with the laser process and carrying out subsequent analyses, it was found that the films that were immersed in EDC-NHS had higher porosity compared to those that did not undergo this treatment. The spectral analysis revealed that the addition of EDC-NHS promoted a more ordered structure, evidenced by the ratios between the D and G peaks, and a more layered organization, highlighted by the ratios between the 2D and G peaks. Regarding electrical and conductive properties, films that do not contain EDC-NHS showed lower sheet resistance when compared to films with EDC-NHS. This observation suggests that the combination of genipin and EDC-NHS may not be the most suitable for optimizing electrical conductivity. Among the 4 films analyzed, the Gel-Gen-NaB-EDC film presented conductive characteristics closest to those of natural cardiac tissue, highlighting its potential in biomedical applications. This film had a conductivity of $(0.8 \pm 0.2)$ S/m, while natural cardiac tissue varies between 0.16 S/m longitudinally and 0.005 S/m transversely [63].

Gelatin was chosen as the base material due to its ability to provide a biologically favorable environment for cells [22]. In combination with LIG, which not only has remarkable conductive properties but is also eco-friendly, anisotropic conductive topographies can be created [13].

This study showed that the substrate Gel-Gen-NaB-EDC has a high potential as the preferred option for the culture of iPSC-CMs. This substrate demonstrated greater compatibility and cell viability, a morphology more aligned with mature CMs, high cell proliferation and indications of maturation and functionality of iPSC-CMs. Additionally, it stood out for the organization and density of the $\alpha$-Actinin aggregations, as well as the clear visualization of its cell nuclei.

Considering the findings made, several possible directions for future investigations emerge. The good performance of the Gel-Gen-NaB-EDC film suggests the possibility of advancing the electrical stimulation of iPSC-CMs on this substrate, which could further enhance their functionality.

Subsequent studies could explore the different compositions of the genipin film, such as adjusting the concentration of genipin or incorporating other elements, aiming to optimize the environment for iPSC-CMs. And given gelatin as a carbon precursor, it would be pertinent to characterize the film before laser treatment using Fourier-transform infrared spectroscopy (FTIR). This analysis would help identify potentially more promising areas for generating LIG since there are intra-sample variations in the chemical composition of the LIG generated.

The combination with emerging technologies, such as three-dimensional printing, opens the door to the development of more sophisticated cardiac tissues and more accurate models for clinical studies. And with the increasing convergence between biology and computing, opportunities arise to create Machine Learning models that predict cellular behaviors on various substrates that have been functionalized with LIG.

In conclusion, this study represents a significant advance in the search for innovative solutions for CVD, exploring the combination of cardiac regeneration, cell therapy and TE. The Gel-Gen-NaB-EDC film stood out as a promising solution, opening new horizons for clinical applications and developments in CTE.

# Bibliography


[1] "Cardiovascular diseases (CVDs)". In: (June 2021). URL: https://www.who.int/news-room/fact-sheets/detail/cardiovascular-diseases-(cvds).

[2] R. Ripa et al. "Physiology, Cardiac Muscle". In: *StatPearls* (July 2023). URL: https://www.ncbi.nlm.nih.gov/books/NBK572070/.

[3] G. V. Novakovic, T. Eschenhagen, and C. Mummery. "Myocardial Tissue Engineering: In Vitro Models". In: *Cold Spring Harbor Perspectives in Medicine* 4 (3 Mar. 2014), a014076. ISSN: 21571422. DOI: 10.1101/CSHPERSPECT.A014076. URL: http://perspectivesinmedicine.cshlp.org/content/4/3/a014076.full.

[4] S. Yamanaka. "Induced pluripotent stem cells: Past, present, and future". In: *Cell Stem Cell* 10 (6 June 2012), pp. 678–684. ISSN: 19345909. DOI: 10.1016/j.stem.2012.05.005. URL: http://www.cell.com/article/S1934590912002378/fulltext.

[5] X. Lian et al. "Directed cardiomyocyte differentiation from human pluripotent stem cells by modulating Wnt/B-catenin signaling under fully defined conditions". In: *Nature Protocols 2013 8:1* 8 (1 Dec. 2012), pp. 162–175. ISSN: 1750-2799. DOI: 10.1038/nprot.2012.150. URL: https://www.researchgate.net/publication/233964178_Directed_cardiomyocyte_differentiation_from_human_pluripotent_stem_cells_by_modulating_Wntb-catenin_signaling_under_fully_defined_conditions.

[6] S. Cho et al. "Reconstructing the heart using iPSCs: Engineering strategies and applications". In: *Journal of molecular and cellular cardiology* 157 (Aug. 2021), p. 56. ISSN: 10958584. DOI: 10.1016/J.YJMCC.2021.04.006. URL: https://www.ncbi.nlm.nih.gov/pmc/articles/PMC8378256/.

[7] I. Karakikes et al. "Human Induced Pluripotent Stem Cell–Derived Cardiomyocytes". In: *Circulation Research* 117 (1 June 2015), pp. 80–88. ISSN: 15244571. DOI: 10.1161/CIRCRESAHA.117.305365. URL: https://www.ahajournals.org/doi/abs/10.1161/circresaha.117.305365.

[8] M. Gherghiceanu et al. "Cardiomyocytes derived from human embryonic and induced pluripotent stem cells: Comparative ultrastructure". In: *Journal of Cellular and Molecular Medicine* 15 (11 Nov. 2011), pp. 2539–2551. ISSN: 15821838. DOI: 10.1111/J.1582-4934.2011.01417.X. URL: https://onlinelibrary.wiley.com/doi/full/10.1111/j.1582-4934.2011.01417.x.

[9] H. T. H. Au et al. "Interactive effects of surface topography and pulsatile electrical field stimulation on orientation and elongation of fibroblasts and cardiomyocytes". In: *Biomaterials* 28 (29 Oct. 2007), p. 4277. ISSN: 01429612. DOI: 10.1016/J.BIOMATERIALS.2007.06.001. URL: https://www.ncbi.nlm.nih.gov/pmc/articles/PMC2039774/.

[10] J. Wang et al. "Graphene Sheet-Induced Global Maturation of Cardiomyocytes Derived from Human Induced Pluripotent Stem Cells". In: *ACS Applied Materials and Interfaces* 9 (31 Aug. 2017), pp. 25929–25940. ISSN: 19448252. DOI: 10.1021/ACSAMI.7B08777/SUPPL_FILE/AM7B08777_SI_008.AVI. URL: https://pubs.acs.org/doi/abs/10.1021/acsami.7b08777.

[11] F. M. Vivaldi et al. "Three-Dimensional (3D) Laser-Induced Graphene: Structure, Properties, and Application to Chemical Sensing". In: *ACS Applied Materials and Interfaces* 13 (26 July 2021), pp. 30245–30260. ISSN: 19448252. DOI: 10.1021/ACSAMI.1C05614/ASSET/IMAGES/LARGE/AM1C05614_0010.JPEG. URL: https://pubs.acs.org/doi/full/10.1021/acsami.1c05614.

[12] J. Lin et al. "Laser-induced porous graphene films from commercial polymers". In: *Nature Communications 2014 5:1* 5 (1 Dec. 2014), pp. 1–8. ISSN: 2041-1723. DOI: 10.1038/ncomms6714. URL: https://www.nature.com/articles/ncomms6714.

[13] L. Huang et al. "Laser-Induced Graphene: En Route to Smart Sensing". In: *Nano-Micro Letters* 12 (1 Aug. 2020), pp. 1–17. ISSN: 21505551. DOI: 10.1007/S40820-020-00496-0/FIGURES/8. URL: https://link.springer.com/article/10.1007/s40820-020-00496-0.

[14] A. F. Carvalho et al. "Laser-Induced Graphene Strain Sensors Produced by Ultraviolet Irradiation of Polyimide". In: *Advanced Functional Materials* 28 (52 Dec. 2018), p. 1805271. ISSN: 1616-3028. DOI: 10.1002/ADFM.201805271. URL: https://proa.ua.pt/index.php/researchua/article/view/23065/16885.

[15] T. Pinheiro et al. "Laser-Induced Graphene on Paper toward Efficient Fabrication of Flexible, Planar Electrodes for Electrochemical Sensing". In: *Advanced Materials Interfaces* 8 (22 Nov. 2021), p. 2101502. ISSN: 2196-7350. DOI: 10.1002/ADMI.202101502. URL: https://onlinelibrary.wiley.com/doi/abs/10.1002/admi.202101502.

[16] L. Li et al. "High-Performance Pseudocapacitive Microsupercapacitors from Laser-Induced Graphene". In: *Advanced Materials* 28 (5 Feb. 2016), pp. 838–845. ISSN: 1521-4095. DOI: 10.1002/ADMA.201503333. URL: https://onlinelibrary.wiley.com/doi/abs/10.1002/adma.201503333.

[17] A. C. Marques et al. "Laser-Induced Graphene-Based Platforms for Dual Biorecognition of Molecules". In: *ACS Applied Nano Materials* 3 (3 Mar. 2020), pp. 2795–2803. ISSN: 25740970. DOI: 10.1021/ACSANM.0C00117/SUPPL_FILE/AN0C00117_SI_001.PDF. URL: https://pubs.acs.org/doi/abs/10.1021/acsanm.0c00117.

[18] A. R. Cardoso et al. "Molecularly-imprinted chloramphenicol sensor with laser-induced graphene electrodes". In: (2018). URL: https://www.sciencedirect.com/science/article/pii/S0956566318308285?casa_token=D8lkQIk54moAAAAA:000Hvn76r_m7pka2sWhiPu8o8Z7c1PWB1Yf2HMomRmemNcrUPh2gpIagBE2rQZCGBIKFWTSjOA.

[19] A. H. Fong et al. "Three-Dimensional Adult Cardiac Extracellular Matrix Promotes Maturation of Human Induced Pluripotent Stem Cell-Derived Cardiomyocytes". In: *https://home.liebertpub.com/tea* 22 (15-16 Aug. 2016), pp. 1016–1025. ISSN: 1937335X. DOI: 10.1089/TEN.TEA.2016.0027. URL: https://www.ncbi.nlm.nih.gov/pmc/articles/PMC4991595/.

[20] H. V. Almeida et al. "Human Extracellular-Matrix Functionalization of 3D hiPSC-Based Cardiac Tissues Improves Cardiomyocyte Maturation". In: *ACS Applied Bio Materials* 4 (2 Feb. 2021), pp. 1888–1899. ISSN: 25766422. DOI: 10.1021/ACSABM.0C01490/ASSET/IMAGES/LARGE/MT0C01490_0004.JPEG. URL: https://pubs.acs.org/doi/full/10.1021/acsabm.0c01490.

[21] D. S. Bergsman et al. "Preserving nanoscale features in polymers during laser induced graphene formation using sequential infiltration synthesis". In: *Nature Communications 2020 11:1* 11 (1 July 2020), pp. 1–8. ISSN: 2041-1723. DOI: 10.1038/s41467-020-17259-5. URL: https://www.nature.com/articles/s41467-020-17259-5.

[22] Y. Jang, Y. Park, and J. Kim. "Engineering Biomaterials to Guide Heart Cells for Matured Cardiac Tissue". In: *Coatings 2020, Vol. 10, Page 925* 10 (10 Sept. 2020), p. 925. ISSN: 2079-6412. DOI: 10.3390/COATINGS10100925. URL: https://www.mdpi.com/2079-6412/10/10/925.

[23] O. Bergmann et al. "Evidence for cardiomyocyte renewal in humans". In: *Science (New York, N.Y.)* 324 (5923 Apr. 2009), pp. 98–102. ISSN: 1095-9203. DOI: 10.1126/SCIENCE.1164680. URL: https://www.ncbi.nlm.nih.gov/pmc/articles/PMC2991140/.

[24] Z. Lin and W. T. Pu. "Strategies for cardiac regeneration and repair". In: *Science translational medicine* 6 (239 June 2014), 239rv1. ISSN: 19466242. DOI: 10.1126/SCITRANSLMED.3006681. URL: https://www.ncbi.nlm.nih.gov/pmc/articles/PMC4280908/.

[25] O. Caspi et al. "Transplantation of Human Embryonic Stem Cell-Derived Cardiomyocytes Improves Myocardial Performance in Infarcted Rat Hearts". In: *Journal of the American College of Cardiology* 50 (19 Nov. 2007), pp. 1884–1893. ISSN: 07351097. DOI: 10.1016/j.jacc.2007.07.054.

[26] C. Fischer et al. "Long-term functional and structural preservation of precision-cut human myocardium under continuous electromechanical stimulation in vitro". In: *Nature Communications 2019 10:1* 10 (1 Jan. 2019), pp. 1–12. ISSN: 2041-1723. DOI: 10.1038/s41467-018-08003-1. URL: https://www.nature.com/articles/s41467-018-08003-1.

[27] D. R. Amin et al. "Nanomaterials for Cardiac Tissue Engineering". In: *Molecules 2020, Vol. 25, Page 5189* 25 (21 Nov. 2020), p. 5189. ISSN: 1420-3049. DOI: 10.3390/MOLECULES25215189. URL: https://www.mdpi.com/1420-3049/25/21/5189/htm.

[28] P. J. Gouveia et al. "Flexible nanofilms coated with aligned piezoelectric microfibers preserve the contractility of cardiomyocytes". In: *Biomaterials* 139 (Sept. 2017), pp. 213–228. ISSN: 0142-9612. DOI: 10.1016/J.BIOMATERIALS.2017.05.048. URL: https://www.sciencedirect.com/science/article/pii/S0142961217303848.

[29] Q. A. Majid et al. "Natural Biomaterials for Cardiac Tissue Engineering: A Highly Biocompatible Solution". In: *Frontiers in Cardiovascular Medicine* 7 (Oct. 2020), p. 554597. ISSN: 2297055X. DOI: 10.3389/FCVM.2020.554597/BIBTEX. URL: https://www.frontiersin.org/articles/10.3389/fcvm.2020.554597/full?field=&id=554597&journalName=Frontiers_in_Cardiovascular_Medicine&utm_campaign=Email_publication&utm_content=T1_11.5e1_author&utm_medium=Email&utm_source=Email_to_authors_.

[30] A. H. Nguyen et al. "Cardiac tissue engineering: state-of-the-art methods and outlook". In: *Journal of Biological Engineering 2019 13:1* 13 (1 June 2019), pp. 1–21. ISSN: 1754-1611. DOI: 10.1186/S13036-019-0185-0. URL: https://jbioleng.biomedcentral.com/articles/10.1186/s13036-019-0185-0.

[31] A. Vashisth et al. "ReaxFF Simulations of Laser-Induced Graphene (LIG) Formation for Multifunctional Polymer Nanocomposites". In: *ACS Applied Nano Materials* 3 (2 Feb. 2020), pp. 1881–1890. ISSN: 25740970. DOI: 10.1021/ACSANM.9B02524/SUPPL_FILE/AN9B02524_SI_002.MPG. URL: https://pubs.acs.org/doi/abs/10.1021/acsanm.9b02524.

[32] S. Dudala et al. "Electromicrofluidic device with integrated PDMS microchannel and laser-induced graphene electrodes for electrochemical detection of cardiac biomarker in a point-of-care platform". In: *Journal of Micromechanics and Microengineering* 32 (10 Aug. 2022), p. 104001. ISSN: 0960-1317. DOI: 10.1088/1361-6

439/AC8A55. URL: https://iopscience.iop.org/article/10.1088/1361-6439/ac8a55.

[33] T. Vićentić et al. "Laser-Induced Graphene for Heartbeat Monitoring with HeartPy Analysis". In: *Sensors 2022, Vol. 22, Page 6326* 22 (17 Aug. 2022), p. 6326. ISSN: 1424-8220. DOI: 10.3390/S22176326. URL: https://www.mdpi.com/1424-8220/22/17/6326/htm.

[34] K. Settu, P. T. Chiu, and Y. M. Huang. "Laser-Induced Graphene-Based Enzymatic Biosensor for Glucose Detection". In: *Polymers 2021, Vol. 13, Page 2795* 13 (16 Aug. 2021), p. 2795. ISSN: 2073-4360. DOI: 10.3390/POLYM13162795. URL: https://www.mdpi.com/2073-4360/13/16/2795/htm.

[35] W. T. Wang et al. "One-step laser induced conversion of a gelatin-coated polyimide film into graphene: Tunable morphology, surface wettability and microsupercapacitor applications". In: *Science China Technological Sciences* 64 (5 May 2021), pp. 1030–1040. ISSN: 18691900. DOI: 10.1007/S11431-020-1609-4/METRICS. URL: https://link.springer.com/content/pdf/10.1007/s11431-020-1609-4.pdf.

[36] C. Larrigy et al. "Porous 3D Graphene from Sustainable Materials: Laser Graphitization of Chitosan". In: *Advanced Materials Technologies* 8 (4 Feb. 2023), p. 2201228. ISSN: 2365-709X. DOI: 10.1002/ADMT.202201228. URL: https://onlinelibrary.wiley.com/doi/full/10.1002/admt.202201228.

[37] M. G. Haugh, M. J. Jaasma, and F. J. O'Brien. "The effect of dehydrothermal treatment on the mechanical and structural properties of collagen-GAG scaffolds". In: *Journal of Biomedical Materials Research Part A* 89A (2 May 2009), pp. 363–369. ISSN: 1552-4965. DOI: 10.1002/JBM.A.31955. URL: https://repository.rcsi.com/articles/journal_contribution/The_effect_of_dehydrothermal_treatment_on_the_mechanical_and_structural_properties_of_collagen-GAG_scaffolds_/10764695/2.

[38] H. G. Sundararaghavan et al. "Genipin-induced changes in collagen gels: correlation of mechanical properties to fluorescence". In: *Journal of biomedical materials research. Part A* 87 (2 Nov. 2008), pp. 308–320. ISSN: 1552-4965. DOI: 10.1002/JBM.A.31715. URL: https://sites.rutgers.edu/david-shreiber/wp-content/uploads/sites/116/2020/02/Sundararaghavan_et_al-2008-Journal_of_Biomedical_Materials_Research_Part_A.pdf.

[39] H. Park et al. "Electronic Functionality Encoded Laser-Induced Graphene for Paper Electronics". In: *ACS Applied Nano Materials* 3 (7 July 2020), pp. 6899–6904. ISSN: 25740970. DOI: 10.1021/acsanm.0c01255. URL: https://pubs.acs.org/doi/full/10.1021/acsanm.0c01255?casa_token=nYGgJ6_IfYEAAAAA%3A_G9R__HRwl11vE6ujA9odp9gDqk15007NuqaajERSmBjGK2IZp5anDHEmB-EJxVgcWtPYkq1GtxByYw.

[40] Y. Chyan et al. "Laser-Induced Graphene by Multiple Lasing: Toward Electronics on Cloth, Paper, and Food". In: *ACS Nano* 12 (3 Mar. 2018), pp. 2176–2183. ISSN: 1936086X. DOI: 10.1021/ACSNANO.7B08539/ASSET/IMAGES/LARGE/NN-2017-08539V_0007.JPEG. URL: https://pubs.acs.org/doi/full/10.1021/acsnano.7b08539.

[41] P. I. Pedro et al. *Sustainable carbon sources for green laser-induced graphene: A perspective on fundamental principles, applications, and challenges*. Dec. 2022. DOI: 10.1063/5.0100785. URL: https://pubs.aip.org/aip/apr/article/9/4/041305/2835381.

[42] M. J. Nine et al. "Graphene-Borate as an Efficient Fire Retardant for Cellulosic Materials with Multiple and Synergetic Modes of Action". In: *ACS Applied Materials and Interfaces* 9 (11 Mar. 2017), pp. 10160–10168. ISSN: 19448252. DOI: 10.1021/acsami.7b00572. URL: https://pubs.acs.org/doi/full/10.1021/acsami.7b00572?casa_token=vVuXTjAiRRYAAAAA%3AqQ3970RIieTaxoUFJhNY6H5Hwtn84j6PzlVXM19WQPyLMEOm4H80bWhcA7UBEdBUBS1WqwQBhODqZnY.

[43] Z. A. Nagieb, M. A. Nassar, and M. G. El-Meligy. "Effect of Addition of Boric Acid and Borax on Fire-Retardant and Mechanical Properties of Urea Formaldehyde Saw Dust Composites". In: *International Journal of Carbohydrate Chemistry* 2011 (Nov. 2011), pp. 1–6. ISSN: 1687-9341. DOI: 10.1155/2011/146763. URL: https://www.hindawi.com/journals/ijcc/2011/146763/.

[44] X. Chen et al. "Effect of the Application of a Dehydrothermal Treatment on the Structure and the Mechanical Properties of Collagen Film". In: *Materials* 13 (2 Jan. 2020). ISSN: 19961944. DOI: 10.3390/MA13020377. URL: https://www.ncbi.nlm.nih.gov/pmc/articles/PMC7013574/.

[45] Z. Wang et al. "Regeneration of skeletal system with genipin crosslinked biomaterials". In: *Journal of Tissue Engineering* 11 (2020). ISSN: 20417314. DOI: 10.1177/2041731420974861. URL: https://www.ncbi.nlm.nih.gov/pmc/articles/PMC7705197/.

[46] J. M. Ruijgrok, J. R. de Wijn, and M. E. Boon. "Glutaraldehyde crosslinking of collagen: Effects of time, temperature, concentration and presoaking as measured by shrinkage temperature". In: *Clinical Materials* 17 (1 Jan. 1994), pp. 23–27. ISSN: 0267-6605. DOI: 10.1016/0267-6605(94)90044-2. URL: https://link.springer.com/content/pdf/10.1007/BF00121695.pdf.

[47] Z. Ahmad et al. "Effect of 1-ethyl-3-(3-dimethylaminopropyl) carbodiimide and N-hydroxysuccinimide concentrations on the mechanical and biological characteristics of cross-linked collagen fibres for tendon repair". In: *Regenerative Biomaterials* 2 (2 June 2015), p. 77. ISSN: 20563426. DOI: 10.1093/RB/RBV005. URL: https://www.ncbi.nlm.nih.gov/pmc/articles/PMC4669024/.

[48] H. V. Almeida et al. "Anisotropic Shape-Memory Alginate Scaffolds Functionalized with Either Type I or Type II Collagen for Cartilage Tissue Engineering". In: *Tissue engineering. Part A* 23 (1-2 Jan. 2017), pp. 55–68. ISSN: 1937335X. DOI: 10.1089/TEN.TEA.2016.0055. URL: https://www.researchgate.net/publication/308946340_Anisotropic_Shape-Memory_Alginate_Scaffolds_Functionalized_with_Either_Type_I_or_Type_II_Collagen_for_Cartilage_Tissue_Engineering.

[49] *Laser System VLS3.50: Cutting and Engraving Machine | CENIMAT*. URL: https://www.cenimat.fct.unl.pt/services/laboratory-electronic-and-optoelectronic-materials-and-devices/laser-system-vls350-cutting-and-engraving-machine.

[50] *Raman Microscope – Renishaw Qontor | CENIMAT*. URL: https://www.cenimat.fct.unl.pt/services/laboratory-electronic-and-optoelectronic-materials-and-devices/raman-microscope-renishaw-qontor.

[51] *Biorad/Nanometrics HL5500 Hall effect systems | CENIMAT*. URL: https://www.cenimat.fct.unl.pt/lab-facilities/electrical-characterization-lab/biorad/nanometrics-hl5500-hall-effect-systems.

[52] *Scanning Electron Microscope - Environmental Health and Safety - Purdue University*. URL: https://www.purdue.edu/ehps/rem/laboratory/equipment%20safety/Research%20Equipment/sem.html.

[53] *Tabletop microscope TM3030 Plus Hitachi | CENIMAT*. URL: https://www.cenimat.fct.unl.pt/lab-facilities/nanofabrication-lab/tabletop-microscope-tm3030-plus-hitachi.

[54] G. Höflinger. *Brief Introduction to Coating Technology for Electron Microscopy*. Aug. 2013. URL: https://www.leica-microsystems.com/science-lab/life-science/brief-introduction-to-coating-technology-for-electron-microscopy/.

[55] *Optical Stereo Microscope - Leica M80 | CENIMAT*. URL: https://www.cenimat.fct.unl.pt/services/laboratory-electronic-and-optoelectronic-materials-and-devices/optical-stereo-microscope-leica-m80.

[56] J. M. Inácio et al. "Gene-Edited Human-Induced Pluripotent Stem Cell Lines to Elucidate DAND5 Function throughout Cardiac Differentiation". In: *Cells* 12 (4 Feb. 2023). ISSN: 20734409. DOI: 10.3390/cells12040520. URL: https://www.mdpi.com/2073-4409/12/4/520.

[57] U. L. S. Team. *VLS Desktop User Guide VLS2.30, VLS3.50*. 2012. URL: https://www.plattsmouth.org/PDF/Library/VLS-Desktop-User-Guide-Rev201208.pdf.

[58] I. Childres et al. *RAMAN SPECTROSCOPY OF GRAPHENE AND RELATED MATERIALS*. 2012. URL: https://www.physics.purdue.edu/quantum/files/Raman_Spectroscopy_of_Graphene_NOVA_Childres.pdf.

[59] Y. Li et al. "Laser-Induced Graphene in Controlled Atmospheres: From Superhydrophilic to Superhydrophobic Surfaces". In: *Advanced materials (Deerfield Beach, Fla.)* 29 (27 July 2017). ISSN: 1521-4095. DOI: 10.1002/ADMA.201700496. URL: https://onlinelibrary.wiley.com/doi/full/10.1002/adma.201700496?casa_token=kZ48EDwOWKUAAAAA%3AZdK7veV3zkgHVb5K46ReR_CdHCZxXApJa-iGw3K4EbAyoquM7xEBcfWMfRT_NgwC1qZ_80gY9RxDc7k.

[60] M. Burke et al. "Fabrication and Electrochemical Properties of Three-Dimensional (3D) Porous Graphitic and Graphenelike Electrodes Obtained by Low-Cost Direct Laser Writing Methods". In: *ACS Omega* 5 (3 Jan. 2020), pp. 1540–1548. ISSN: 24701343. DOI: 10.1021/ACSOMEGA.9B03418/SUPPL_FILE/AO9B03418_SI_001.PDF. URL: https://pubs.acs.org/doi/epdf/10.1021/acsomega.9b03418.

[61] M. Parmeggiani et al. "PDMS/Polyimide Composite as an Elastomeric Substrate for Multifunctional Laser-Induced Graphene Electrodes". In: (2019). DOI: 10.1021/acsami.9b10408. URL: https://pubs.acs.org/doi/full/10.1021/acsami.9b10408.

[62] F. Mahmood et al. "Laser-Induced Graphene Derived from Kraft Lignin for Flexible Supercapacitors". In: *ACS Omega* 5 (24 June 2020), pp. 14611–14618. ISSN: 24701343. DOI: 10.1021/ACSOMEGA.0C01293. URL: https://pubs.acs.org/doi/epdf/10.1021/acsomega.0c01293.

[63] K. Ashtari et al. "Electrically Conductive Nanomaterials for Cardiac Tissue Engineering". In: *Advanced drug delivery reviews* 144 (Apr. 2019), p. 162. ISSN: 18728294. DOI: 10.1016/J.ADDR.2019.06.001. URL: https://www.ncbi.nlm.nih.gov/pmc/articles/PMC6784829/.

[64] B. Yi, Q. Xu, and W. Liu. "An overview of substrate stiffness guided cellular response and its applications in tissue regeneration". In: *Bioactive Materials* 15 (Sept. 2022), pp. 82–102. ISSN: 2452-199X. DOI: 10.1016/J.BIOACTMAT.2021.12.005. URL: https://www.sciencedirect.com/science/article/pii/S2452199X21005600.

[65] L. D. Wilsbacher and S. R. Coughlin. "Analysis of Cardiomyocyte Development using Immunofluorescence in Embryonic Mouse Heart". In: *Journal of Visualized Experiments : JoVE* (97 Mar. 2015), p. 52644. ISSN: 1940087X. DOI: 10.3791/52644. URL: https://www.ncbi.nlm.nih.gov/pmc/articles/PMC4401388/.

[66] *The cell. 1. Introduction. Cell diversity. Atlas of Plant and Animal Histology*. Apr. 2023. URL: https://mmegias.webs.uvigo.es/02-english/5-celulas/1-diversidad.php.